IL-5-producing CD4+ T cells and eosinophils cooperate to enhance response to immune checkpoint blockade in breast cancer

Blomberg, O.S.; Spagnuolo, L.; Garner, H.; Voorwerk, L.; Isaeva, O.I.; Dyk, E. van; ... ; Kok, M.

Cancer Cell

Article

IL-5-producing CD4$^+$ T cells and eosinophils cooperate to enhance response to immune checkpoint blockade in breast cancer

Graphical abstract

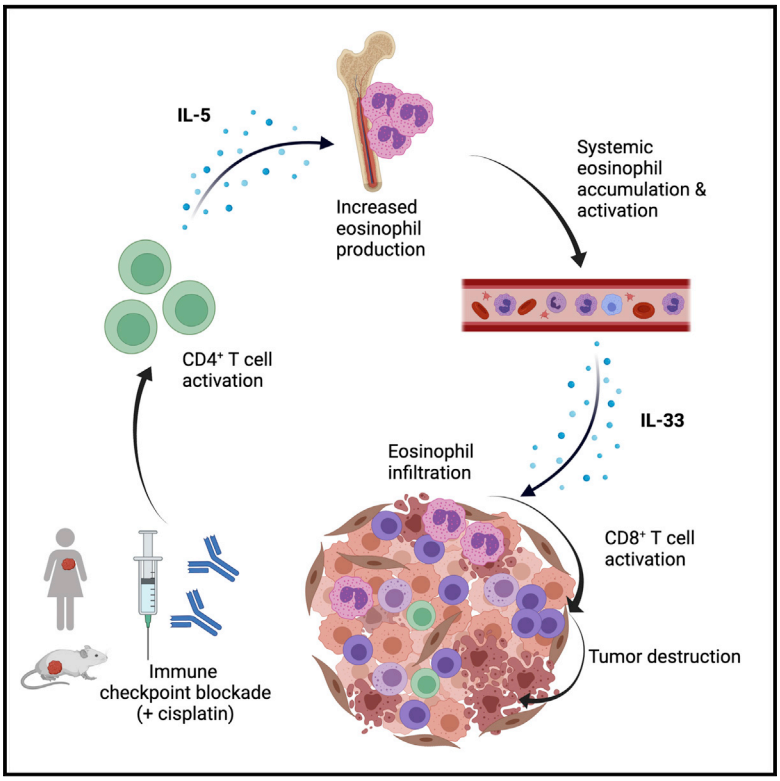

Highlights

- Eosinophils increase in patients with metastatic TNBC who respond to ICB
- Eosinophils are critical for ICB response by enhancing CD8$^+$ T cell activation
- Accumulation of eosinophils is driven by CD4$^+$ T cells, IL-5, and IL-33
- Proof-of-principle evidence for eosinophil engagement to enhance ICB-response

Authors

Olga S. Blomberg, Lorenzo Spagnuolo, Hannah Garner, Leonie Voorwerk, ..., Karin E. de Visser, Marleen Kok

Correspondence

k.d.visser@nki.nl (K.E.d.V.), m.kok@nki.nl (M.K.)

In brief

Immunotherapy is only effective in a proportion of breast cancer patients. Blomberg et al. discover that eosinophils, a myeloid immune cell type, are expanded in responders. They show that eosinophil accumulation depends on CD4$^+$ T cells and eosinophil-stimulating molecules IL-5 and IL-33. Eosinophils enhance activation of CD8$^+$ T cells and improve immunotherapy response.

Blomberg et al., 2023, Cancer Cell *41*, 106–123
January 9, 2023
https://doi.org/10.1016/j.ccell.2022.11.014

CellPress

CellPress
OPEN ACCESS

Cancer Cell

Article

IL-5-producing CD4$^+$ T cells and eosinophils cooperate to enhance response to immune checkpoint blockade in breast cancer

Olga S. Blomberg,[1,2,3,13] Lorenzo Spagnuolo,[1,2,13] Hannah Garner,[1,2,13] Leonie Voorwerk,[1,13] Olga I. Isaeva,[1,4,14] Ewald van Dyk,[1,2,4,14] Noor Bakker,[1,2,14] Myriam Chalabi,[5,6,7] Chris Klaver,[1] Maxime Duijst,[1] Kelly Kersten,[1,11] Marieke Brüggemann,[1] Dorien Pastoors,[1,2,12] Cheei-Sing Hau,[1,2] Kim Vrijland,[1,2] Elisabeth A.M. Raeven,[1,2] Daphne Kaldenbach,[1,2] Kevin Kos,[1,2,3] Inna S. Afonina,[8,9] Paulien Kaptein,[5] Louisa Hoes,[2,5,7] Willemijn S.M.E. Theelen,[10] Paul Baas,[10] Emile E. Voest,[2,5,7] Rudi Beyaert,[8,9] Daniela S. Thommen,[5] Lodewyk F.A. Wessels,[2,4] Karin E. de Visser,[1,2,3,15,16,*] and Marleen Kok[1,7,15,*]

[1]Division of Tumor Biology & Immunology, The Netherlands Cancer Institute, Amsterdam, the Netherlands
[2]Oncode Institute, Utrecht, the Netherlands
[3]Department of Immunology, Leiden University Medical Centre, Leiden, the Netherlands
[4]Division of Molecular Carcinogenesis, The Netherlands Cancer Institute, Amsterdam, the Netherlands
[5]Division of Molecular Oncology & Immunology, The Netherlands Cancer Institute, Amsterdam, the Netherlands
[6]Department of Gastrointestinal Oncology, The Netherlands Cancer Institute, Amsterdam, the Netherlands
[7]Department of Medical Oncology, The Netherlands Cancer Institute, Amsterdam, the Netherlands
[8]VIB-UGent Center for Inflammation Research, Ghent University, Ghent, Belgium
[9]Department of Biomedical Molecular Biology, Ghent University, Ghent, Belgium
[10]Department of Thoracic Oncology, The Netherlands Cancer Institute, Amsterdam, the Netherlands
[11]Present address: Department of Pathology, University of California San Francisco, San Francisco, CA, USA
[12]Present address: Department of Hematology, Erasmus University Medical Center, Rotterdam, the Netherlands
[13]These authors contributed equally
[14]These authors contributed equally
[15]These authors contributed equally
[16]Lead contact
*Correspondence: k.d.visser@nki.nl (K.E.d.V.), m.kok@nki.nl (M.K.)
https://doi.org/10.1016/j.ccell.2022.11.014

SUMMARY

Immune checkpoint blockade (ICB) has heralded a new era in cancer therapy. Research into the mechanisms underlying response to ICB has predominantly focused on T cells; however, effective immune responses require tightly regulated crosstalk between innate and adaptive immune cells. Here, we combine unbiased analysis of blood and tumors from metastatic breast cancer patients treated with ICB with mechanistic studies in mouse models of breast cancer. We observe an increase in systemic and intratumoral eosinophils in patients and mice responding to ICB treatment. Mechanistically, ICB increased IL-5 production by CD4$^+$ T cells, stimulating elevated eosinophil production from the bone marrow, leading to systemic eosinophil expansion. Additional induction of IL-33 by ICB-cisplatin combination or recombinant IL-33 promotes intratumoral eosinophil infiltration and eosinophil-dependent CD8$^+$ T cell activation to enhance ICB response. This work demonstrates the critical role of eosinophils in ICB response and provides proof-of-principle for eosinophil engagement to enhance ICB efficacy.

INTRODUCTION

Immune checkpoint blockade (ICB) has emerged in the last decade as an effective strategy for the treatment of multiple cancer types. However, in metastatic breast cancer, durable responses are only seen in approximately 5% of the patients and are mainly limited to triple-negative breast cancer (TNBC).[1,2] While response rates can be increased by selecting patients with PD-L1$^+$ tumors or by combining ICB with chemotherapy,[3,4] most breast cancer patients do not benefit from ICB. A better understanding of the mechanisms that underlie response to ICB is crucial for the rational design of immunomodulatory strategies.

Research into the mechanisms of response to ICB has predominantly focused on T cells; however, an effective immune response requires tightly regulated crosstalk between adaptive and innate immune cells.[5] One innate immune cell type gaining increasing attention in the context of anti-tumor immunity is the eosinophil.[6,7] Eosinophils are bone marrow-derived granulocytes involved in

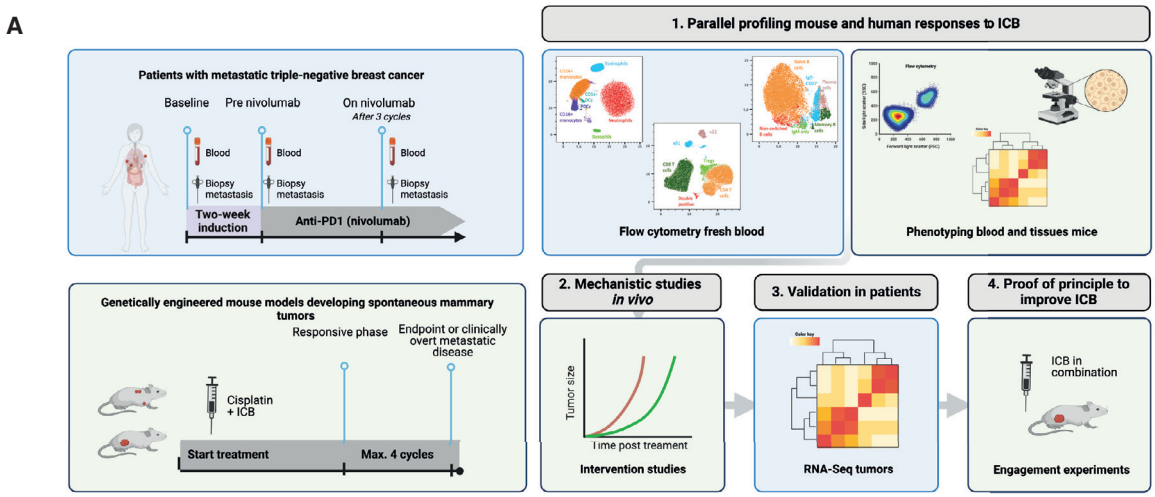

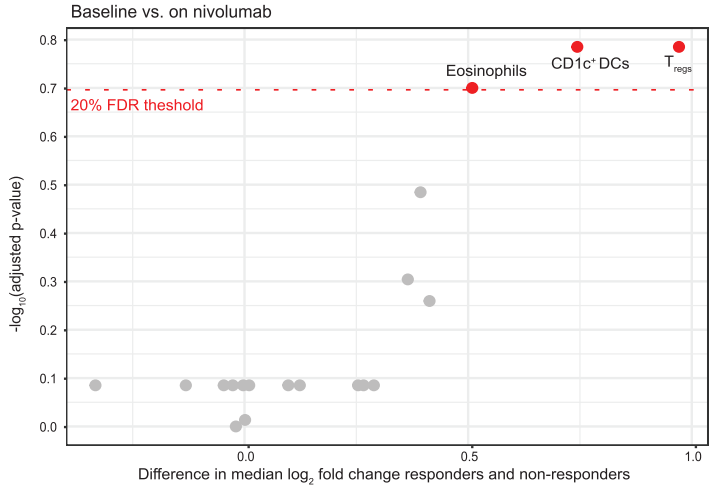

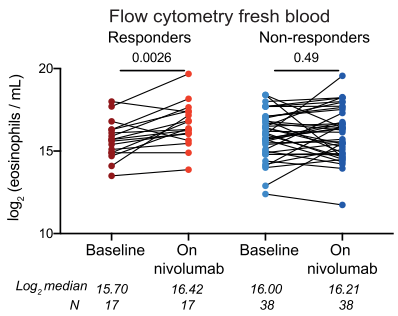

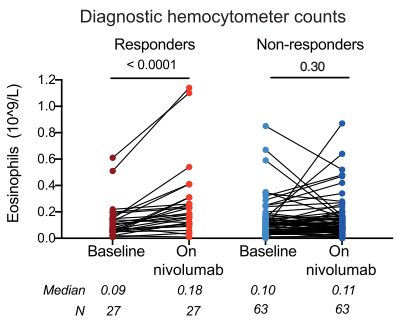

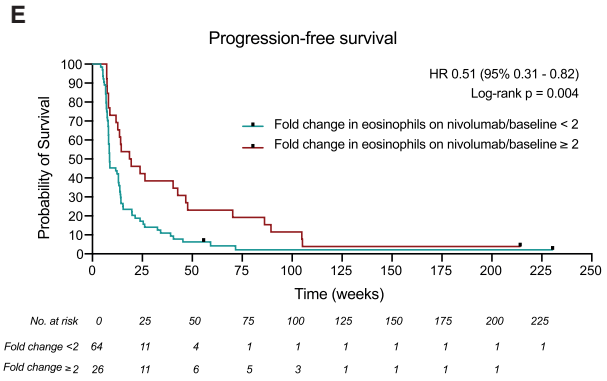

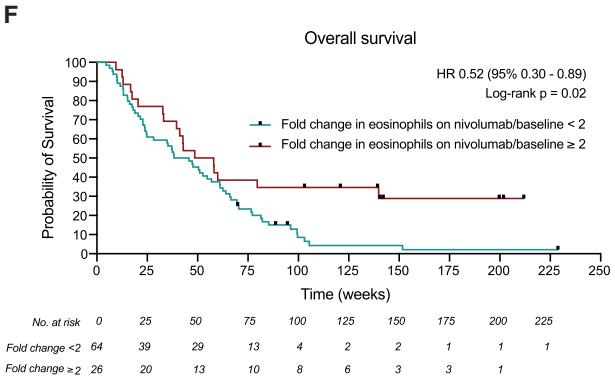

(legend on next page)

tissue homeostasis and repair, parasite clearance, and the pathophysiology of various diseases, including allergic asthma and autoimmunity.[8] In the context of cancer, opposing functions of eosinophils have been reported depending on cancer type and disease stage.[9–18] Recently, eosinophils have emerged as unexpected players in an effective response to ICB. Increased eosinophil levels during ICB treatment correlate with response to PD-1-, PD-L1-, or CTLA-4-targeting antibodies in patients with metastatic melanoma,[19–21] non-small cell lung cancer (NSCLC),[22,23] and renal cell carcinoma (RCC).[24] Whether eosinophils are associated with response to ICB in patients with less immunogenic cancer types, such as breast cancer, remains to be elucidated. Moreover, it is critical to assess whether eosinophils merely serve as a biomarker or are causally involved in ICB response. Preclinical studies point toward a functional involvement of eosinophils in anti-tumor immunity[11–14] and eosinophils were also recently reported to promote intratumoral vessel normalization and anti-tumor immunity upon CTLA-4 blockade.[25] Nonetheless, their role in ICB response remains poorly understood. Furthermore, the mechanisms leading to eosinophil accumulation and recruitment to the tumor upon ICB are still unknown.

In this study, we combined unbiased analyses of the systemic immune landscape upon ICB in patients with metastatic TNBC with in-depth mechanistic studies in spontaneous mouse models of primary and metastatic breast cancer (Figure 1A), which mimic the poorly immunogenic and highly immunosuppressive characteristics of human breast cancer.[26,27] We uncover a critical role for eosinophils during ICB response and elucidate the mechanisms that lead to systemic eosinophil expansion and tumor infiltration.

RESULTS

Increase in circulating eosinophils in patients responding to ICB

To assess response-related changes in the systemic immune landscape of patients with metastatic breast cancer, we set up an immunomonitoring pipeline of fresh blood by high-dimensional flow cytometry (Figure 1A). We profiled patients with metastatic TNBC treated with anti-PD-1 (nivolumab) enrolled in a phase II clinical trial (TONIC trial, n = 111, Figures S1A and S1B; characteristics in Tables S1 and S2).[28] Patients were treated with nivolumab alone or with nivolumab following a 2-week induction period with either low-dose chemotherapy, irradiation, or a 2-week waiting period (Figure S1A). Blood samples were analyzed by flow cytometry at baseline (before induction treatment), after induction treatment (pre-nivolumab) and after three cycles of nivolumab (on-nivolumab). Extensive analysis of individual time points did not reveal predictive immune cell populations that could distinguish responders from non-responders (Figures S1C–S1E). However, when analyzing the dynamics of immune cell populations upon ICB treatment by comparing baseline with on-nivolumab, we identified three differentially regulated immune cell populations associated with response: $CD1c^+$ dendritic cells (DCs), regulatory T cells (T_{regs}), and eosinophils (Figures 1B and S1F). We observed a decrease in $CD1c^+$ DCs in non-responding patients (Figure S2A). In contrast, eosinophils and T_{regs} were increased upon ICB specifically in responders (Figures 1C, S2B, and S2C). The same three populations emerged when we compared the pre-nivolumab (post-induction) with on-nivolumab time points, indicating that the induction treatments did not significantly change the dynamics of these immune populations (Figures S2D–S2F). In light of recent reports of systemic eosinophil expansion correlating with ICB response in several tumor types,[19–24] we further investigated the increase in eosinophils associated with response to ICB.

To validate our results in a technically independent manner we evaluated circulating eosinophil counts using routine hemocytometer analysis (Figure S1B for sample overlap with flow cytometry samples). We confirmed that circulating eosinophils significantly increase in responders on-nivolumab, compared with both baseline and pre-nivolumab (Figures 1D and S2G–S2H). Importantly, patients with increased circulating eosinophils upon treatment had longer progression-free survival (Figures 1E and S2I) and overall survival (Figures 1F and S2J), underscoring the clinical relevance of an eosinophil increase in ICB response.

To evaluate whether increased eosinophils during ICB response extends beyond breast cancer, NSCLC,[22,23] RCC,[24] and melanoma,[19–21] we investigated eosinophil counts in patients treated with ICB in other phase II clinical trials at The Netherlands Cancer Institute. Comparing patients responding to ICB with non-responders, we observed a significantly higher fold change in circulating eosinophils in patients with advanced NSCLC (Figures S3A and S3B; PEMBRO-RT trial[29]) and in patients with early-stage mismatch repair-proficient (pMMR) colon cancer (CC) (Figures S3C and S3D; NICHE trial[30]). No statistically significant difference in paired eosinophil counts could be seen upon ICB in patients with mismatch repair-deficient (dMMR) cancers (Figures S3E and S3G; NICHE trial and dMMR cohort DRUP trial[30,31]), suggesting that an eosinophil increase might be less relevant in highly immunogenic tumors. In summary, we demonstrate that eosinophils accumulate systemically upon ICB response in three independent cohorts of patients with metastatic TNBC, metastatic NSCLC, or early-stage pMMR CC, emphasizing that systemic eosinophil expansion is a common feature of ICB response across multiple cancer types.

Figure 1. ICB response in metastatic TNBC patients is associated with systemic eosinophil expansion

(A) Schematic overview of study design. Created with Biorender.com.

(B) Volcano plot depicting the difference in median $\log_2$ fold change from baseline to on-nivolumab between responding and non-responding patients with metastatic TNBC (TONIC trial, NCT02499367) and adjusted p values for systemic immune cell populations (cells/mL) analyzed by flow cytometry.

(C and D) Paired analysis of circulating eosinophils at baseline versus on-nivolumab by flow cytometry ($\log_2$ transformed cells/mL) (C) and by hemocytometer analysis (D). Wilcoxon signed-rank test.

(E and F) Kaplan-Meier curve of progression-free survival (E) or overall survival (F) of patients according to the fold change in eosinophils (baseline to on-nivolumab) lower than 2 or equal to/higher than 2. Log rank and univariate hazard ratios by Cox regression (fold change lower than 2 as reference category). See also Figures S1–S3 and Tables S1 and S2.

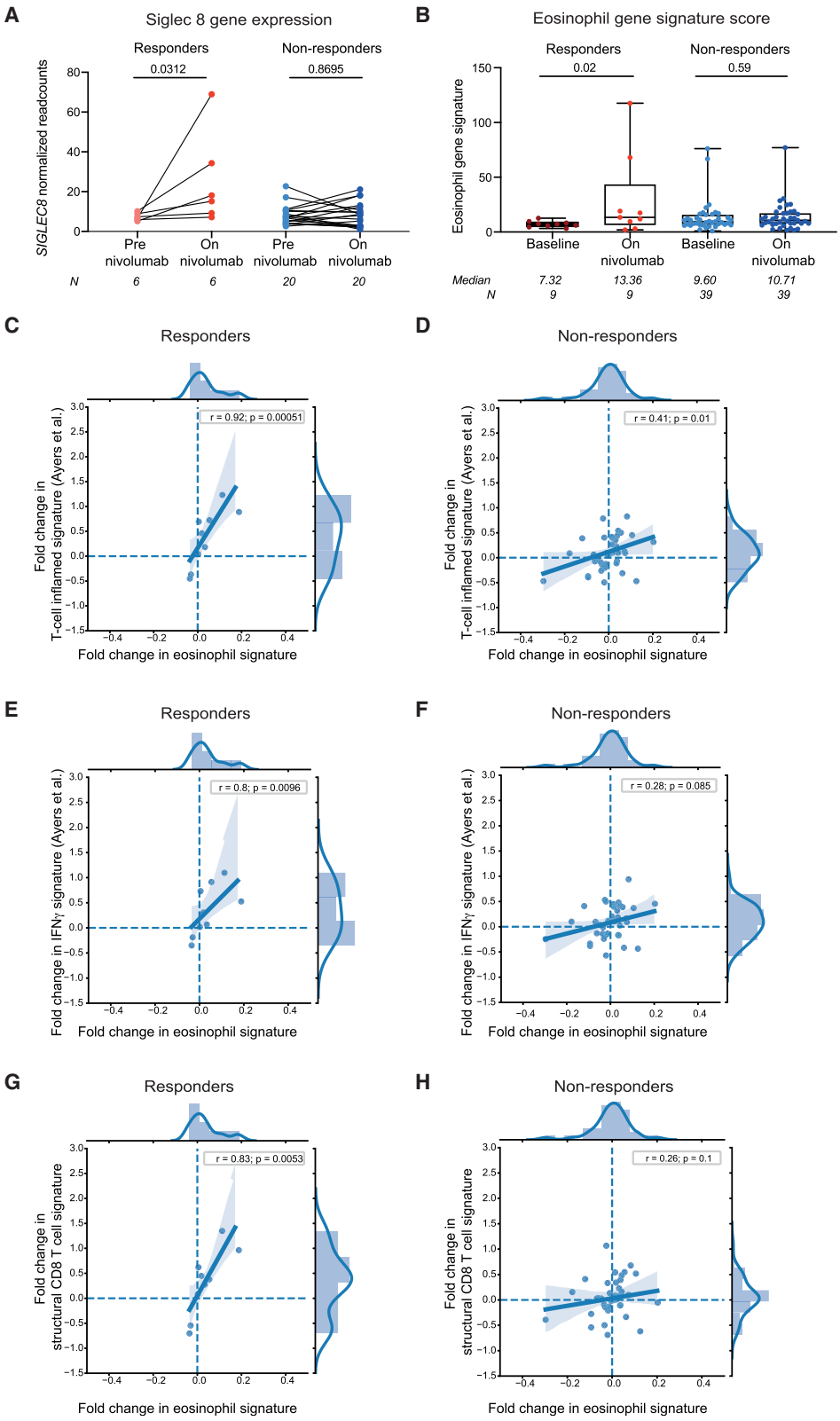

Figure 2. ICB response in TNBC patients is associated with increased intratumoral eosinophil-related gene expression

(A) Paired intratumoral *SIGLEC8* normalized read counts from NanoString IO360 gene expression analysis from pre-nivolumab and on-nivolumab biopsies. Wilcoxon signed-rank test.

(legend continued on next page)

Increase of intratumoral eosinophil-related gene expression correlates with response to ICB and increased CD8$^+$ T cell signatures

To assess whether eosinophils accumulate intratumorally upon ICB, we evaluated the expression of *SIGLEC8* in paired metastases obtained at baseline and during nivolumab treatment of TNBC patients (TONIC trial, NanoString IO360 panel, sample availability, Figure S1B). SIGLEC8 is a marker expressed at high levels on human eosinophils and mast cells and to a lower degree on basophils.[32] We detected a statistically significant increase in *SIGLEC8* upon ICB in tumors from responders but not in non-responders (Figure 2A). To complement this analysis, we applied an eosinophil signature containing genes highly expressed by eosinophils to the RNA sequencing dataset (Table S3). Intratumoral expression of these genes increased upon ICB in responders but not in non-responders (Figure 2B). Using this signature, we assessed whether elevation in intratumoral eosinophils is accompanied by an intratumoral increase in (activated) CD8$^+$ T cells, as shown for metastatic melanoma.[19] We applied a widely used T cell inflamed gene signature,[33] an IFN-γ signature,[33] and a structural CD8$^+$ T cell signature consisting of genes related to the CD8$^+$ T cell receptor complex (Table S3). We observed a significant correlation between increased expression upon ICB of eosinophil-related genes and all three T cell-related gene signatures in metastatic lesions of responders, and not in non-responders (Figures 2C–2H). Together, our results indicate that response to ICB associates with an increase in circulating eosinophils and an increase of eosinophil-related genes in the tumor microenvironment. This increase in eosinophil-related genes correlates with increased CD8$^+$ T cell-related genes, suggesting a potential connection between eosinophils and CD8$^+$ T cell activation during an effective ICB response.

ICB synergizes with cisplatin and induces eosinophil accumulation in spontaneous primary and metastatic breast cancer models

Our clinical observations raise the question whether eosinophil expansion is a bystander effect of ICB response, or whether eosinophils are functionally involved. To probe the causality between eosinophil dynamics and outcome after ICB in breast cancer, we used the *Keratin14-cre;Cdh1$^{F/F}$;Trp53$^{F/F}$* (KEP) mouse model for *de novo* mammary tumorigenesis[34] (Figure 3A) and the KEP-based mastectomy model for spontaneous multi-organ metastatic disease[35] (Figures 3B, S4A, and S4B). KEP mice bearing established mammary tumors did not respond to blockade of PD-1 and CTLA-4 (referred to as ICB; Figure 3C). Similarly, metastasis-bearing mice did not respond to ICB alone (Figure 3D), recapitulating the poor response to ICB observed in metastatic breast cancer patients. Platinum-based drugs synergize with ICB in preclinical models[36,37] due to their beneficial immunomodulatory effects,[38,39] in line with improved response rates when ICB is combined with chemotherapy in metastatic TNBC patients.[3,4] While combining cisplatin with either anti-PD-1 or anti-CTLA-4 was insufficient to improve the survival benefit provided by cisplatin (Figure S4C), the combination of cisplatin with anti-PD-1 and anti-CTLA-4 (CIS + ICB) resulted in extension of survival of KEP mice (Figure 3C) and led to durable responses in mice bearing established metastases (Figure 3D). The therapeutic synergy between CIS + ICB was characterized by a systemic increase in effector CD44$^+$CD62L$^-$ T cells and increased expression of activation markers and cytokines, such as IFN-γ and TNF-α, by both CD4$^+$ and CD8$^+$ T cells (Figures S4D and S4E). Depletion of CD8$^+$ T cells abrogated the synergistic effect observed upon CIS + ICB in mammary tumor-bearing KEP mice (Figure 3C), confirming a critical role of CD8$^+$ T cells as effector cells in CIS + ICB therapy.

In addition to increased T cell activation, in-depth profiling of the immune landscape of primary tumors, metastases, and blood by flow cytometry of both models revealed that only eosinophils consistently increased in frequency upon CIS + ICB therapy (Figures 3E–3H). While ICB induced accumulation of circulating eosinophils (Figures 3E and 3F), increased eosinophil infiltration in primary tumors and metastatic lesions was only observed when ICB was combined with cisplatin (Figures 3G and H). In addition, we observed an increase in eosinophils in the tumor-draining lymph node (TDLN) and spleen of KEP mice treated with CIS + ICB (Figure S4F). Immunohistochemical staining for major basic protein (MBP), a granular protein specifically expressed by eosinophils, confirmed that the increase in eosinophils in primary KEP tumors was only achieved upon CIS + ICB (Figure S4G).

To evaluate whether treatment with CIS + ICB also influences the phenotype of eosinophils, we performed RNA sequencing on eosinophils sorted from blood of metastasis-bearing mice during the responsive phase of therapy, namely 21 days after initiation of treatment. We observed 858 differentially expressed genes (fold change $\geq$1 and $p \leq 0.05$) in eosinophils from CIS + ICB-treated mice compared with control antibody-treated mice (Figure S4H). Gene set enrichment analysis identified IFN-γ response as the top hit among the immune-related pathways enriched in eosinophils upon CIS + ICB (Figures S4I–S4J). Other immune-related pathways included TGF-β signaling, TNF-α signaling via NF-κB, IL6-JAK-STAT3 signaling, and inflammatory response (Figure S4I). Moreover, we observed enrichment of the oxidative phosphorylation pathway in eosinophils from control antibody-treated compared with combination-treated mice (Figure S4K). These observations indicate that, in CIS + ICB-treated mice, eosinophils are not only increased in number, but also phenotypically altered. Collectively, these data demonstrate that ICB synergizes with cisplatin resulting in improved survival and is associated with systemic and intratumoral expansion of eosinophils, in line with our clinical observations.

(B) Mean of normalized expression values of eosinophil signature genes from paired biopsies of metastases as assessed by RNA sequencing analysis. Boxplots display minimum and maximum values (whiskers), interquartile range (box) with median. Wilcoxon signed-rank test.
(C–H) Correlation between the fold change (baseline to on-nivolumab) in an eosinophil gene signature described in (B) and the fold change (baseline to on-nivolumab) in a T cell inflamed gene signature (expanded immune gene signature of Ayers et al.[33]) (C and D), a structural CD8$^+$ T cell gene signature (E and F), or an IFN-γ gene signature[33] (G and H) in responders (left) and non-responders (right). Lines with colored field represent the regression line with 95% confidence interval, including histogram and kernel density estimates. Spearman's correlation coefficient. See also Table S3.

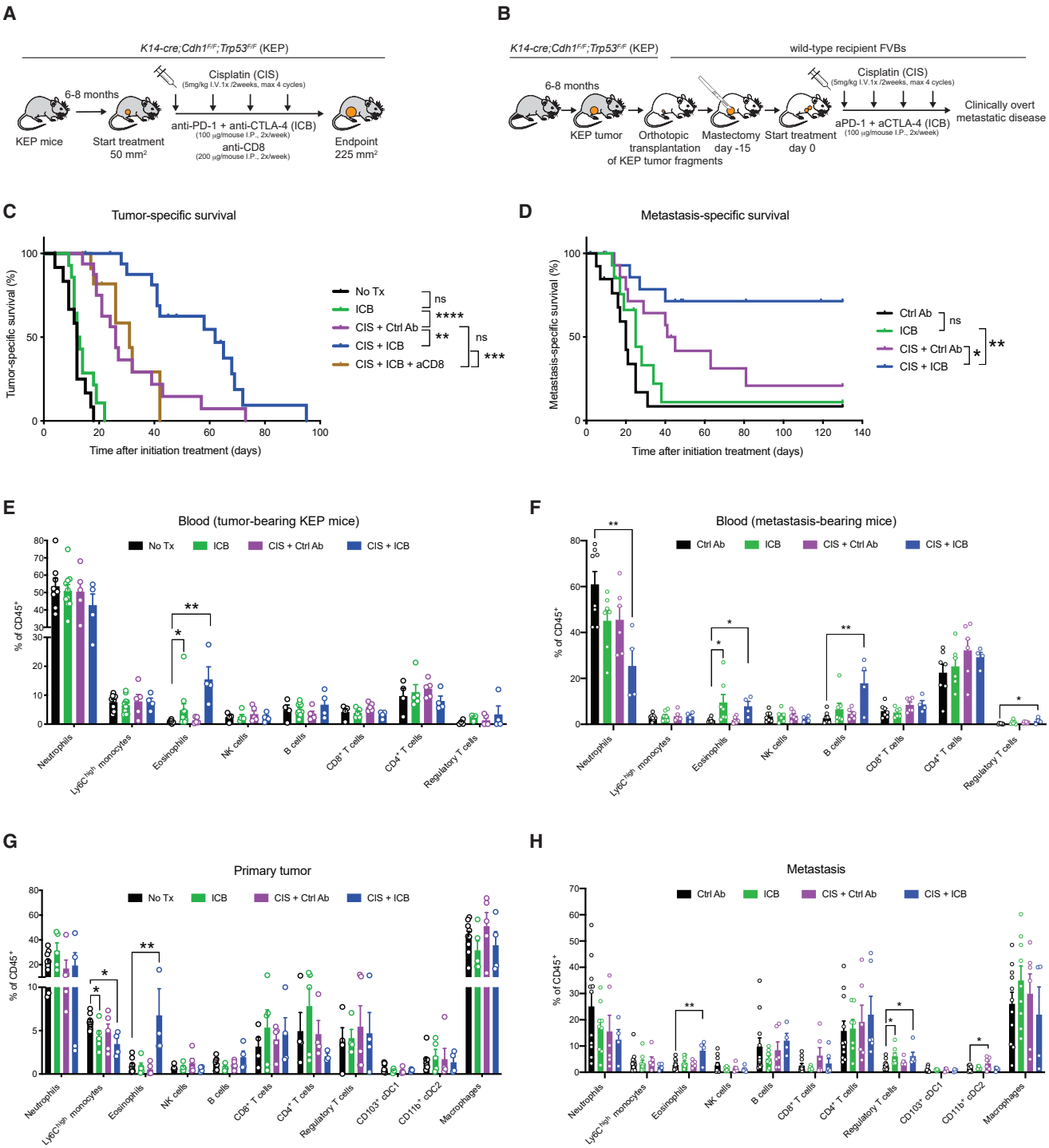

Figure 3. ICB synergizes with cisplatin and induces eosinophil expansion in mouse models

(A and B) Experimental setup of transgenic KEP model (A) and KEP-based metastasis model (B) including treatment schemes.

(C) Kaplan-Meier survival curves of KEP mice treated as indicated (untreated, No Tx, n = 12; ICB, n = 14, 1 censored; CIS + Ctrl Ab, n = 17, 2 censored; CIS + ICB, n = 18, 5 censored; CIS + ICB + anti-CD8, n = 12, 4 censored). Tumor-related endpoint was defined as cumulative tumor burden of 225 mm^2.

(D) Kaplan-Meier survival curves of metastasis-bearing mice treated as indicated (control antibody, Ctrl Ab, n = 13, 1 censored; ICB, n = 15, 5 censored; CIS + Ctrl Ab, n = 15, 3 censored; CIS + ICB, n = 16, 7 censored). Metastasis-related endpoint was defined as mice displaying signs of respiratory distress caused by metastatic disease or when lymph node metastasis reached the size of 225 mm^2. Censored events are mice sacrificed for weight loss (C and D) or local recurrence of the mastectomized tumor (D). Log rank (Mantel-Cox) test.

(E and F) Frequency of immune cell populations in the blood of KEP mice at tumor-related endpoint (E) or metastasis-bearing mice at metastasis-related endpoint (F) as determined by flow cytometry.

(legend continued on next page)

Eosinophil depletion abrogates CD8$^+$ T cell activation and ICB response

To elucidate whether CIS + ICB-induced eosinophilia is critical for the observed therapeutic benefit, we depleted eosinophils with an antibody targeting SiglecF.[11,12,25,40,41] Anti-SiglecF treatment effectively depleted eosinophils without altering other immune cells, including neutrophils (Figures S5A–S5C). In line with the literature,[42] we observed a subset of SiglecF$^+$ neutrophils in our tumor models (5%–20% of intratumoral neutrophils, data not shown). However, the expression levels of SiglecF on these neutrophils was lower than on eosinophils (Figure S5D). To exclude the possibility that anti-SiglecF treatment depletes SiglecF$^+$ neutrophils, we quantified Ly6G$^+$ (neutrophils) and MBP$^+$ (eosinophils) cells by immunohistochemical staining. The total number of neutrophils was unaffected by anti-SiglecF treatment, whereas eosinophils were effectively depleted (Figures S5E and S5F). Importantly, eosinophils were also effectively depleted during anti-SiglecF treatment in combination with cisplatin +/− ICB (Figures 4A and S5G).

The administration of anti-SiglecF alone did not affect KEP tumor growth (Figure S5H). Strikingly, depletion of eosinophils abrogated the synergistic effect observed between CIS + ICB, while depletion of eosinophils had no effect on therapeutic benefit of cisplatin alone (Figures 4B–4D). Similarly, depletion of eosinophils completely abrogated the synergistic effect of CIS + ICB in metastasis-bearing mice, but had no effect on the efficacy of cisplatin alone (Figure 4E). These findings reveal a causal role for eosinophils in the synergistic effect of CIS + ICB therapy, both in primary and metastatic breast cancer models.

Because the synergistic effect of CIS + ICB is dependent on both CD8$^+$ T cells and eosinophils, we hypothesized that eosinophils play a role in inducing intratumoral CD8$^+$ T cell infiltration or activation. It was previously shown that eosinophils can promote T cell activation and recruitment into tumors,[11,13,18,25,40] and we observed an association between intratumoral eosinophils and CD8$^+$ T cells in responding patients with advanced breast cancer (Figures 2C–2H). To test this hypothesis, we analyzed the immune landscape of KEP tumors during the responsive phase of therapy. Intratumoral CD8 counts increased upon treatment with cisplatin compared with control antibody but did not further increase upon addition of ICB. Importantly, CD8 counts were not dependent on the presence of eosinophils (Figure 4F). Instead, eosinophil depletion completely reverted the increased activation of intratumoral CD8$^+$ T cells induced by CIS + ICB, most notably in terms of CD44 expression and IFN-γ production (Figures 4G and 4H). These data demonstrate that eosinophils are essential for increased intratumoral CD8$^+$ T cell activation during CIS + ICB therapy.

In addition, CD4 and FOXP3 cell counts increased upon cisplatin treatment compared with control, but did not change further upon CIS + ICB and was independent of eosinophil presence (Figures S5I and S5J). While CIS + ICB also increased the intratumoral frequency of effector CD44$^+$ CD4$^+$ T cells, this was independent of eosinophils (Figures S5K–S5N), demonstrating that eosinophils specifically affect intratumoral CD8$^+$ T cell activation. Interestingly, we also observed a higher frequency of CD44$^+$ and IFN-γ^+ CD8$^+$ T cells in the TDLN upon CIS + ICB that was abrogated upon eosinophil depletion (Figure S5O). In contrast, the frequency of CD44$^+$ CD4$^+$ T cells or CD44$^+$ T_{regs} in TDLN was not increased by combination treatment nor affected by eosinophil depletion (Figures S5P and S5Q). Collectively, these observations show that eosinophils are critical for the therapeutic action of CIS + ICB, by facilitating CD8$^+$ T cell activation in the tumor and TDLN.

IL-5 is required for ICB-induced eosinophil accumulation and therapeutic benefit

To investigate how ICB mediates the systemic eosinophil increase, we analyzed metastasis-bearing mice at different time points during the metastatic cascade and treatment. The eosinophil frequency in the blood increased after 7 days of ICB treatment and was maintained at high levels until at least 21 days (Figure S6A). Concomitantly, we observed an increase in eosinophils in the bone marrow (Figure 5A) and an increase of Lin$^-$Sca1$^-$CD34$^+$cKit^{Int}CD125$^+$Gr1$^-$ cells, which have been described previously as eosinophil progenitors (Figures 5B and S6B).[43] Furthermore, both immature (cKit^{int}CCR3^{low}) and fully mature (cKit$^-$CCR3$^+$) eosinophils increased in the bone marrow upon ICB (Figures 5C–5E), while all other hematopoietic progenitor and immune cell populations remained unaffected (Figure S6C). Altogether, these observations suggest that the systemic increase of eosinophils induced by ICB is caused by increased eosinophil production in the bone marrow.

To assess which systemic factors induced by ICB could promote eosinophil production in the bone marrow, followed by systemic eosinophil accumulation, we measured the expression of a panel of cytokines in the plasma of metastatic mice. Strikingly, the only significantly increased cytokine upon ICB was IL-5 (Figures 5F and S6D), which is a major eosinophil regulator.[44] To investigate whether ICB treatment in human tumors induces IL-5 upregulation, we made use of the patient-derived tumor fragment (PDTF) platform.[45] This platform allows interrogation of the early immunological response of human tumor tissues upon *ex vivo* ICB treatment (aPD1 and combined aPD1 + aCTLA4). Importantly, the observed *ex vivo* response (defined as described previously[45,46]) correlates with the clinical response of the patient.[45] We assessed the protein levels of IL-5 upon *ex vivo* ICB stimulation in tumors of patients with different tumor types. We observed an increase in IL-5 expression specifically in tumors that showed an immunological response to *ex vivo* ICB (PDTF-R) compared with non-responding tumors (PDTF-NR), both upon aPD1 alone and combined aPD1 + aCTLA4 treatment (Figures 5G; Table S4), demonstrating that IL-5 can be induced in human tumors by ICB.

To assess whether IL-5 drives eosinophil expansion upon ICB in metastasis-bearing mice, we blocked IL-5 using a neutralizing antibody. Indeed, the number of eosinophils in bone marrow, blood, and (pre-)metastatic lungs was drastically reduced (Figures 5H–5J). Importantly, ICB did not promote an eosinophil

(G and H) Frequency of immune cell populations in the primary tumor of KEP mice at tumor-related endpoint (G) or metastatic lesions of mice at metastasis-related endpoint (H) as determined by flow cytometry. Eosinophils were defined CD11b$^+$Ly6G^{low}SiglecF$^+$SSC^{high} in blood and CD11b$^+$Ly6G^{low}SiglecF$^+$F4/80^{int} in tumor. Mean ± SEM. One-way ANOVA or Kruskal-Wallis followed by Dunnett's or Dunn's multiple comparisons test, comparing each group against control-treated mice. *$p < 0.05$, **$p < 0.01$, ***$p < 0.001$, ****$p < 0.0001$. See also Figure S4.

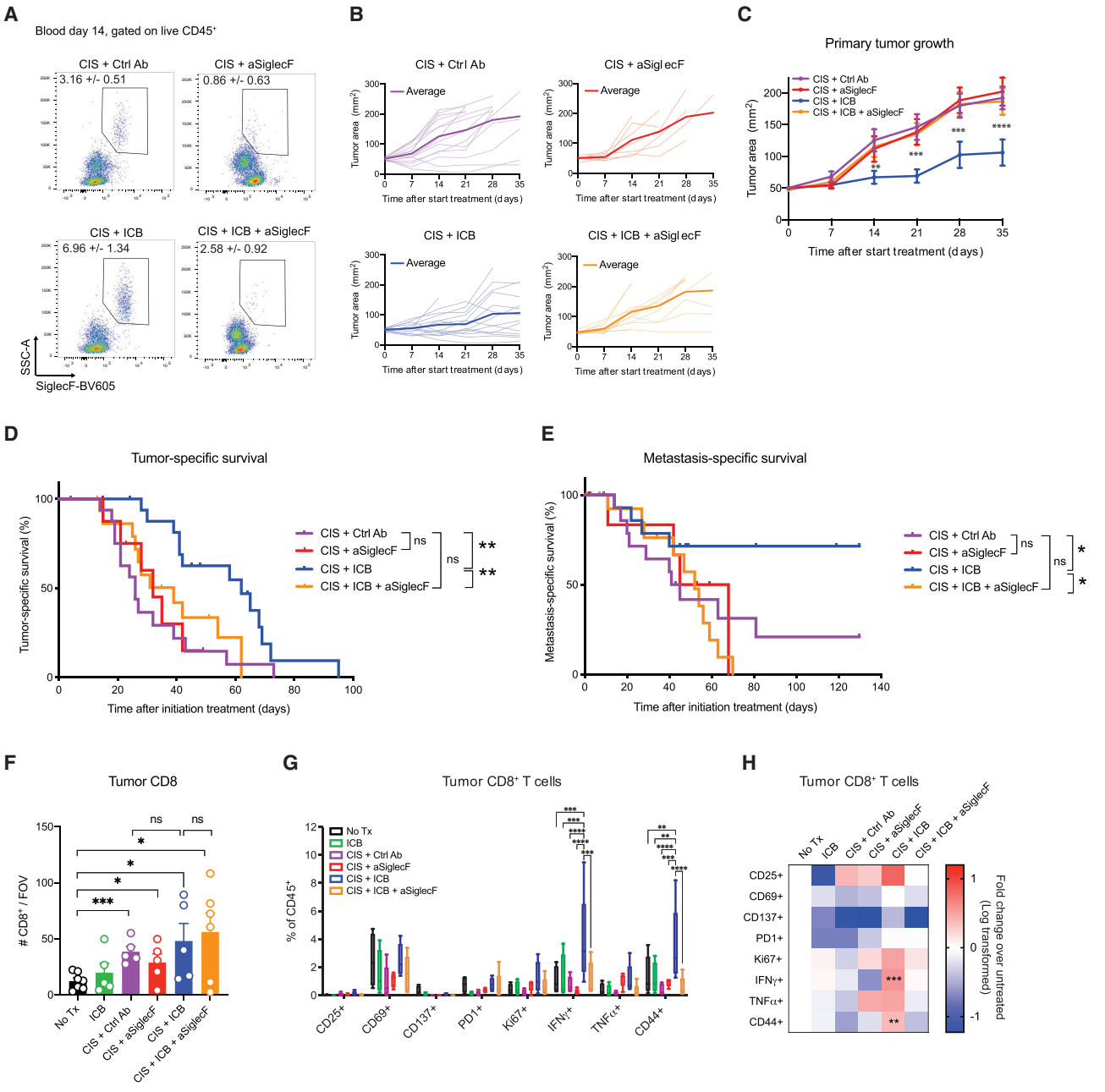

Figure 4. Eosinophils are critical for ICB-cisplatin response via CD8+ T cell activation

(A) Representative dot plots showing eosinophil levels in blood of KEP mice 14 days after start of indicated treatments. Mean frequency of eosinophils as percentage of CD45+ cells ± SEM is displayed.

(B) Individual (light) and average (dark) tumor growth curves of KEP mice treated as indicated.

(C) Average growth curve ± SEM of the aforementioned treatment groups. Two-way ANOVA followed by Dunnett's multiple comparisons test.

(D) Kaplan-Meier survival curves of KEP mice treated as indicated (CIS + Ctrl Ab, same curve as in Figure 3C); CIS + anti-SiglecF, n = 8, 2 censored; CIS + ICB, same curve as in Figure 3C; CIS + ICB + anti-SiglecF, n = 18, 5 censored). Log rank (Mantel-Cox) test.

(E) Kaplan-Meier survival curves showing metastasis-related survival of mice treated as indicated (CIS + Ctrl Ab, same curve as in Figure 3D; CIS + anti-SiglecF, n = 6, 2 censored, CIS + ICB, same curve as in Figure 3D; CIS + ICB + anti-SiglecF, n = 19, 7 censored). Log rank (Mantel-Cox) test.

(F) Number of tumor-infiltrating CD8+ T cells quantified by IHC (n = 5–7 mice per group, average of 5–9 high-power microscopic fields per mouse). KEP mice were treated as described in Figure 3A and analyzed 21 days after start of treatment or when tumors reached an area of 225 mm^2. Mean ± SEM, Student's t test.

(G) Frequency of indicated activation markers expressed on intratumoral CD8+ T cells upon different treatments, determined by flow cytometry (n = 4–5). Boxes represent median and interquartile range; whiskers full range. Two-way ANOVA followed by Tukey's multiple comparison test.

(H) Data of (G) were normalized to the frequency observed in control mice. Log transformed data are presented. ns, not significant; *p < 0.05, **p < 0.01, ***p < 0.001, ****p < 0.0001. See also Figure S5.

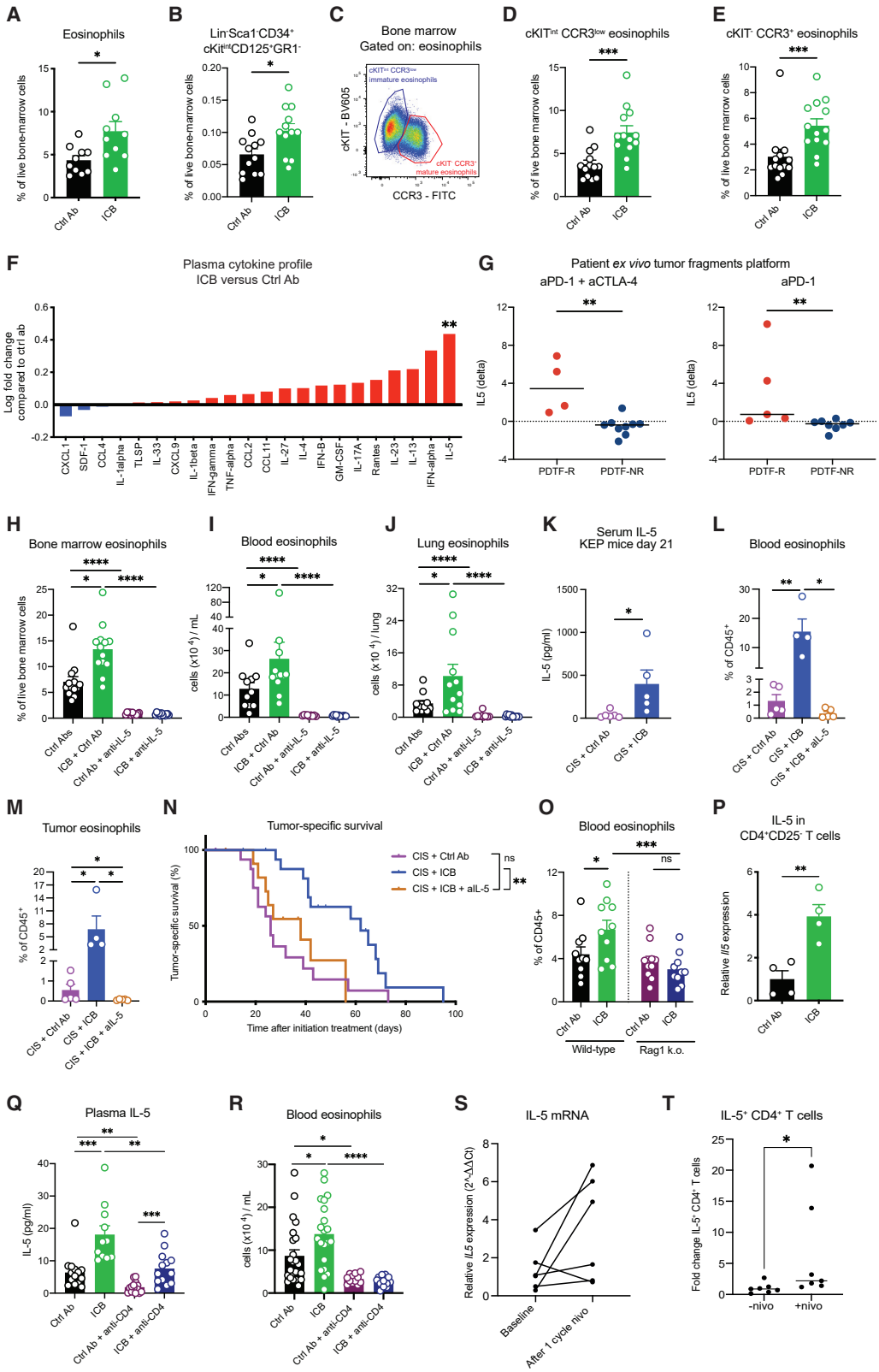

(legend on next page)

increase after IL-5 blockade in any of the organs analyzed, indicating that ICB-induced eosinophils are IL-5 dependent. In line with our observations in metastasis-bearing mice, serum IL-5 levels were similarly increased in tumor-bearing KEP mice during the responsive phase of CIS + ICB therapy (Figure 5K). IL-5 blockade during CIS + ICB therapy in KEP mice reduced eosinophil levels both systemically and intratumorally (Figures 5L and 5M), without affecting other myeloid cells (Figures S6E and S6F). Importantly, anti-IL-5 treatment abolished the therapeutic benefit induced by CIS + ICB (Figure 5N), phenocopying the effect of anti-SiglecF-induced eosinophil depletion (Figure 4D). Collectively, these findings demonstrate that IL-5 is a key driver of eosinophil accumulation and therapeutic benefit of CIS + ICB therapy.

IL-5-producing CD4$^+$ T cells drive eosinophil production and systemic expansion upon ICB

IL-5 can be produced by various cell types, principally CD4$^+$ T cells, type 2 innate lymphoid cells (ILC2s) and other innate immune cells, such as mast cells and eosinophils.[44] To evaluate whether adaptive or innate immune cells are needed to induce eosinophils upon ICB, we treated KEP tumor-bearing wild-type and *Rag-1*-deficient mice, which lack mature B and T cells but retain ILC2s and myeloid cells, with ICB or control antibody. Importantly, ICB failed to induce an increase in eosinophils in tumor-bearing *Rag*-1-deficient mice (Figure 5O), indicating that adaptive immune cells trigger eosinophil expansion upon ICB. Based on these findings, we hypothesized that CD4$^+$ T cells are the main source of IL-5 upon ICB, and thus cause eosinophilia. Indeed, we observed increased expression of *IL-5* mRNA in circulating CD4$^+$CD25$^-$ T cells upon ICB in metastasis-bearing mice (Figure 5P). Depletion of CD4$^+$ T cells reduced plasma IL-5 levels and the number of eosinophils in bone marrow and blood of metastasis-bearing mice (Figures 5Q, 5R, and S6G), suggesting a role for CD4$^+$ T cells in eosinophil homeostasis. Importantly, in the absence of CD4$^+$ T cells, there was reduced induction of IL-5 by ICB (Figure 5Q). Notably, ICB treatment still induced a slight but significant increase of serum IL-5 in CD4$^+$ T cell-depleted mice compared with controls (Figures 5Q and S6G), suggesting other sources of IL-5, such as ILC2s, mast cells, and eosinophils, may produce the residual IL-5. Importantly, in line with the reduced induction of IL-5 upon ICB in the absence of CD4$^+$ T cells, systemic eosinophil numbers did not increase upon ICB in CD4$^+$ T cell-depleted mice (Figures 5R and S6H). In addition to mature bone marrow eosinophils, the frequency of Lin$^-$Sca1$^-$CD34$^+$cKit^{Int}CD125$^+$Gr1$^-$ eosinophil progenitors did not increase upon ICB after CD4$^+$ T cell depletion (Figure S6I). These data demonstrate that CD4$^+$ T cells are required for the ICB-induced increase in systemic IL-5 levels, eosinophil production in the bone marrow, and systemic eosinophil accumulation. Importantly, CD4$^+$ T cell depletion also reduced the number of circulating eosinophils in metastasis-bearing mice treated with CIS + ICB (Figure S6J), confirming that CD4$^+$ T cells are required for eosinophil increase not only upon ICB treatment alone but also during CIS + ICB. To exclude the potential contribution of T_{regs} in ICB-induced eosinophilia, we used KEP tumor-bearing *Foxp3$^{-DTR-GFP}$* mice allowing specific depletion of FOXP3 expressing T_{regs} (Figures S6K and S6L).[47] Upon T_{reg} depletion, blood eosinophil numbers during ICB were further increased compared with T_{reg}-proficient mice (Figure S6M), indicating that T_{regs} do not facilitate ICB-induced eosinophil expansion, but hamper ICB-induced eosinophilia.

To address whether CD4$^+$ T cells are a source of IL-5 in TNBC patients, we utilized peripheral blood mononuclear cells

Figure 5. CD4$^+$ T cell-derived IL-5 is required for ICB-induced eosinophil expansion and therapeutic benefit

(A–E) KEP metastasis-bearing mice were treated as indicated (Ctrl Ab, n = 10–13; ICB, n = 10–13) and sacrificed 10 days after start of treatment. Frequency of total eosinophils (live Lin$^-$CD127$^-$CD11b$^+$CD115$^-$SiglecF$^+$) (A), live Lin$^-$Sca1$^-$CD34$^+$cKit^{Int}CD125$^+$Gr1$^-$ eosinophil progenitors (B), representative dot plot (C), and quantification of cKit^{int}CCR3^{low} (D), and cKit$^-$CCR3$^+$ (E) eosinophils in bone marrow as determined by flow cytometry.

(F) Relative expression of the indicated cytokines in the plasma of mice treated as described above (Ctrl Ab n = 9, ICB n = 10), determined by LEGENDplex, and normalized to Ctrl Ab-treated mice.

(G) Fold change in IL-5 secretion by PDTF treated *ex vivo* with aPD-1+aCTLA-4 (left) or aPD-1 (right) compared with untreated condition, measured by LEGENDplex, comparing PDTF-R (responders) and PDTF-NR (non-responders), defined as described previously.[45,46] Tumor samples were collected from surgical material of patients with various tumor types (see STAR Methods and Table S4).

(H–J) Metastasis-bearing mice were treated with IgG2a and IgG1 control antibodies (Ctrl Abs, n = 14), ICB + IgG1 (n = 14), IgG2a + anti-IL-5 (n = 11), or ICB + anti-IL-5 (n = 12) and analyzed 10 days after start of treatment. Number of eosinophils in bone marrow (H), blood (I), and lungs (J) determined by flow cytometry. Lung eosinophils were defined as CD45$^+$CD11b$^+$Ly6G$^-$SiglecF$^+$F4/80^{int}.

(K) IL-5 levels in serum of tumor-bearing KEP mice analyzed 21 days after start of the indicated treatments measured by ELISA.

(L and M) Frequency of eosinophils in the blood (L) and tumor (M) of KEP mice treated as indicated and analyzed at tumor-related endpoint as determined by flow cytometry (n = 4–5). Data from CIS + Ctrl Ab and CIS + ICB are the same mice as in Figure 3G.

(N) Kaplan-Meier survival curves of KEP mice treated as indicated (CIS + Ctrl Ab, same curve as in Figure 3C; CIS + ICB, same curve as in Figure 3C; CIS + ICB + anti-IL-5, n = 12, 3 censored). Log rank (Mantel-Cox) test.

(O) Number of eosinophils in blood of wild-type (WT) or *Rag1* knockout (KO) mice with KEP-derived orthotopic mammary tumors, treated as indicated (Ctrl Ab, WT n = 10, *Rag1* KO n = 10; ICB, WT = 10, *Rag1* KO n = 10), analyzed by flow cytometry when tumors reached an area of 144 mm^2.

(P) *Il5* gene expression in CD4$^+$CD25$^-$ T cells sorted from blood of metastasis-bearing mice treated as indicated (Ctrl Ab n = 4, ICB n = 4), determined by qRT-PCR. Relative expression to Ctrl Ab-treated mice is shown.

(Q and R) Metastasis-bearing mice were treated with isotype control antibodies (Ctrl Ab, n = 13–25), ICB (n = 13–21), Ctrl Ab + anti-CD4 (n = 14), or ICB + anti-CD4 (n = 13), and sacrificed 10 days after start of treatment.

(Q) Plasma IL-5 levels measured by ELISA.

(R) Number of eosinophils in the blood, as determined by flow cytometry. Pooled data of two independent experiments.

(S) *IL5* gene expression determined by qRT-PCR in CD4$^+$ T cells sorted from PBMCs at baseline and after one cycle of nivolumab of metastatic TNBC patients treated in the control arm of the TONIC trial (n = 6).

(T) Fold change in frequency of IL-5$^+$ CD4$^+$ T cells among total CD4$^+$ T cells from TNBC patients (n = 7) treated *ex vivo* with aPD1 compared with untreated conditions, measured by intracellular flow cytometry. All data are mean ± SEM, statistical analysis by unpaired t test or Mann-Whitney, unless differently indicated. ns, not significant; *p < 0.05, **p < 0.01, ***p < 0.001, ****p < 000.1. See also Figure S6 and Table S4.

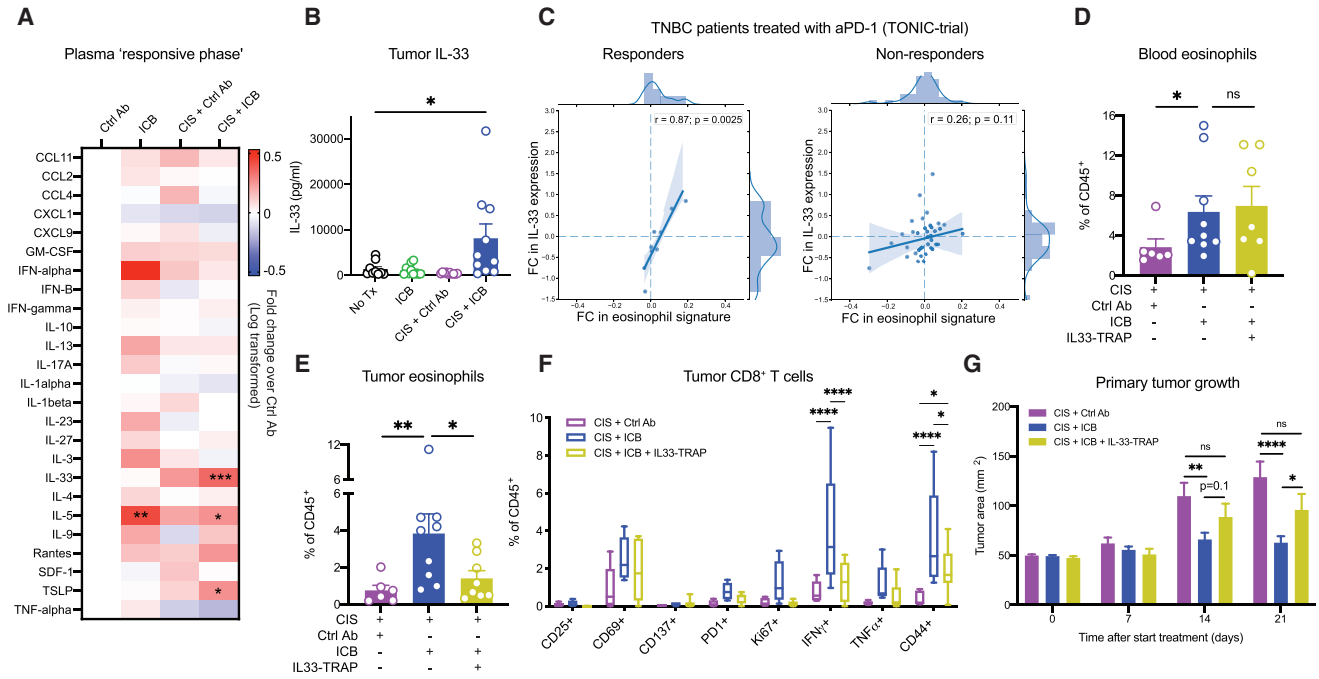

Figure 6. IL-33 drives intratumoral eosinophil infiltration and is required for the therapeutic benefit of CIS + ICB

(A) Relative expression of the indicated cytokines in plasma of metastasis-bearing mice treated as described previously (Ctrl Ab n = 9 [same data as in Figure 5F], ICB n = 10 [same data as in Figure 5F], CIS + Ctrl Ab n = 9, CIS + ICB n = 13), determined by LEGENDplex. Data are normalized to Ctrl Ab-treated mice. One-way ANOVA or Kruskal-Wallis followed by Dunnett's or Dunn's multiple comparisons test, comparing each treatment against control-treated mice, for each cytokine.

(B) IL-33 levels in tumor lysates of end-stage tumors as determined by LEGENDplex (n = 9–10). Mean ± SEM, One-way ANOVA followed by Dunnett's multiple comparisons test, comparing each group against untreated.

(C) Correlation between the fold change (baseline to on-nivolumab) in eosinophil gene signature (described in Figure 2B) and the fold change (baseline to on-nivolumab) in *IL33* in RNA sequencing analysis of paired biopsies from responding (left) and non-responding (right) patients with metastatic TNBC. Graph characteristics as in Figure 2.

(D and E) Frequency of eosinophils in the circulation (D) and tumor (E) of KEP mice analyzed 21 days after start of treatment determined by flow cytometry (n = 6–9). Mean ± SEM, Mann-Whitney.

(F) Frequency of indicated activation markers expressed on intratumoral CD8$^+$ T cells, determined by flow cytometry (n = 5–9). Data from CIS + Ctrl Ab and CIS + ICB are the same mice as in Figure 4G. Boxes represent median and interquartile range; whiskers full range. Two-way ANOVA followed by Tukey's multiple comparison test.

(G) Average tumor growth size ± SEM of KEP mice treated as indicated (CIS + Ctrl Ab n = 23, CIS + ICB n = 32; CIS + ICB + IL33-TRAP n = 12). Mean ± SEM, unpaired t test. ns, not significant; *p < 0.05, **p < 0.01, ***p < 0.001, ****p < 000.1. See also Figures S7A–S7D.

(PBMCs) isolated from patients of the TONIC trial treated with ICB without induction treatment at baseline and after one cycle of nivolumab and performed qRT-PCR for *IL-5* mRNA in sorted CD4$^+$ T cells. Five out of six patients had an increase in *IL-5* transcript in CD4$^+$ T cells upon nivolumab treatment compared with baseline (Figure 5S). To further demonstrate that CD4$^+$ T cells produce IL-5 protein in response to nivolumab, we stimulated PBMCs from TNBC patients with nivolumab for 48 h and analyzed intracellular IL-5 in CD4$^+$ T cells by flow cytometry. These data show a statistically significant fold change in IL-5$^+$ CD4$^+$ T cells upon nivolumab stimulation (Figure 5T), demonstrating that aPD-1 induces IL-5 expression in circulating CD4$^+$ T cells of TNBC patients. Collectively, our data demonstrate that IL-5-producing CD4$^+$ T cells drive eosinophil expansion upon ICB.

IL-33 drives eosinophil recruitment to the TME and is required for the therapeutic benefit of CIS + ICB

Although ICB alone leads to systemic eosinophil accumulation, eosinophil recruitment to the tumor and their subsequent contribution to therapeutic benefit was only observed upon CIS + ICB combination therapy in our preclinical models (Figure 3). We therefore asked which eosinophil-recruiting or activating factors trigger the intratumoral accumulation of eosinophils upon CIS + ICB. Analysis of a broad panel of eosinophil-related cytokines and chemokines revealed that IL-33 was specifically increased upon CIS + ICB in the plasma of metastasis-bearing mice at the responsive phase of therapy (Figure 6A). Similarly, IL-33 levels were increased in tumor lysates and serum of KEP tumor-bearing mice treated with CIS + ICB (Figures 6B and S7A). Importantly, in patients with metastatic TNBC responding to ICB we observed a strong positive correlation between the eosinophil gene signature and *IL-33* expression in metastatic lesions, which was not observed in non-responders, suggesting a link between *IL-33* expression and eosinophil infiltration in the TME (Figure 6C). Of note, in both patients and mice, cisplatin alone was not sufficient to induce a statistically significant increase in IL-33 levels (Figures 6B, S7A, and S7B). IL-33 is an alarmin that amplifies immune responses during inflammation.[48] IL-33 directly promotes eosinophil activation, adhesion, and survival,[49,50] and IL-33

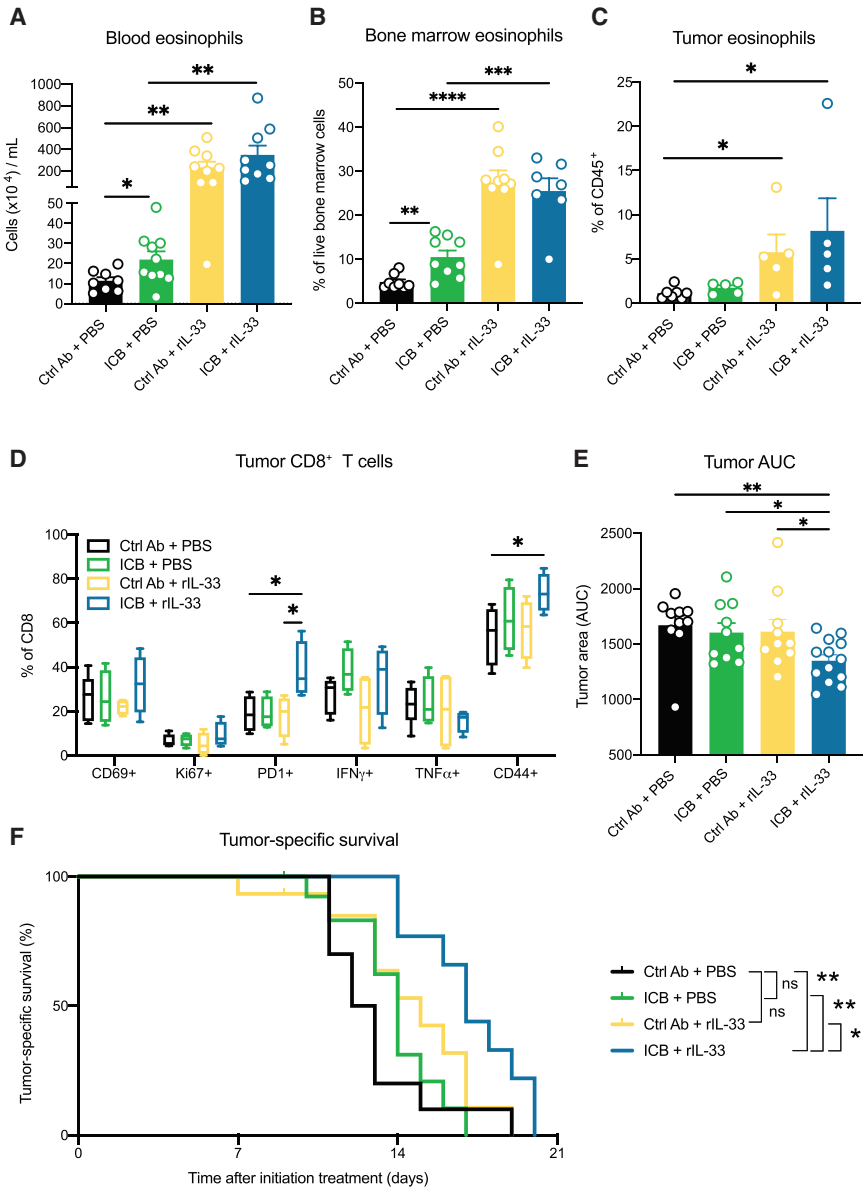

Figure 7. rIL-33 therapy engages eosinophils and enhances ICB response

(A–C) Mice bearing orthotopically transplanted KEP tumors were treated as indicated (Ctrl Ab + PBS, n = 10; ICB + PBS, n = 15; Ctrl Ab + rIL-33, n = 15; ICB + rIL-33, n = 15). Frequency of eosinophils in the circulation (A), bone marrow (B), and tumor (C) were analyzed in the responsive phase of therapy, determined by flow cytometry. Mean ± SEM, t test.

(D) Frequency of indicated activation markers expressed on intratumoral CD8$^+$ T cells in the responsive phase of therapy, determined by flow cytometry (n = 5–7). Boxes represent median and interquartile range; whiskers full range. Two-way ANOVA followed by Tukey's multiple comparison test.

(E) Area under the curve (AUC) of growth curves was determined up to day 14 after start of treatment. Mean ± SEM, one-way ANOVA.

(F) Kaplan-Meier survival curves showing tumor-related survival. Log rank (Mantel-Cox) test. ns, not significant; *p < 0.05, **p < 0.01, ***p < 0.001, ****p < 0.0001. See also Figures S7E and S7F.

contributes to several eosinophilic disorders.[51] In the cancer context, IL-33 has been associated with both pro- and anti-tumor functions.[14,52,53] To assess the functional role of IL-33 in intratumoral eosinophil accumulation, we made use of the IL-33-TRAP fusion protein, a high-affinity IL-33 antagonist.[54] In line with our earlier observation that IL-5 is responsible for ICB-induced systemic eosinophilia (Figure 5), IL-33 neutralization did not affect systemic eosinophil accumulation during CIS + ICB (Figure 6D). However, intratumoral eosinophil infiltration was abrogated upon IL-33 blockade (Figure 6E), indicating that IL-33 is required, directly or indirectly, for eosinophil recruitment to the tumor. IL-33-TRAP also prevented the intratumoral CIS + ICB-induced CD8$^+$ T cell activation without affecting other immune populations (Figures 6F, S7C, and S7D), phenocopying the effect of eosinophil depletion (Figure 4). Importantly, IL-33-TRAP blocked the therapeutic benefit provided by CIS + ICB (Figure 6G). In summary, these data demonstrate that IL-33 is required for eosinophil infiltration in the tumor, CD8$^+$ T cell activation, and therapeutic benefit observed upon ICS + ICB. These preclinical findings are supported by our clinical observation that increased intratumoral eosinophil infiltration is strongly correlated with IL-33 expression as well as to CD8$^+$ T cells in the TME of TNBC patients responding to ICB (Figures 2C–2H and 6C).

Recombinant IL-33 engages eosinophils and enhances response to ICB

In light of our finding that IL-33 drives eosinophil infiltration into the tumor, we hypothesized that deliberate induction of intratumoral accumulation of ICB-educated eosinophils by recombinant IL-33 (rIL-33) might represent a viable strategy to enhance the therapeutic benefit of ICB in breast cancer in the absence of chemotherapy. Treatment of mice bearing orthotopically transplanted KEP tumors with rIL-33 alone or in combination with ICB resulted in increased eosinophils in the blood and bone marrow, as well as increased intratumoral eosinophil infiltration (Figures 7A–7C). However, only the combination of ICB and rIL-33 increased CD8$^+$ T cell activation, and most notably increased the frequency of effector CD44$^+$ and PD-1$^+$ CD8$^+$ T cells (Figure 7D), without altering other immune populations (Figures S7E and S7F). Importantly, IL-33-mediated engagement of eosinophils during ICB and the resulting CD8$^+$ T cell activation was accompanied by improved tumor control and extension of survival (Figures 7E and 7F). Collectively, these data provide proof-of-principle that rIL-33 can engage eosinophils and represents a viable strategy to enhance response to ICB in breast cancer.

DISCUSSION

In this study, we take a translational approach by combining longitudinal analysis of fresh blood and tumor biopsy samples of a patient cohort with functional experiments in clinically relevant mouse models to identify the IL-5- and IL-33-eosinophil axis as crucial mediator of ICB response in breast cancer. The effect of ICB on myeloid cells and the influence of myeloid cells on ICB response is often overlooked. Here, we show that an ICB-induced increase in systemic IL-5, driven by $CD4^+$ T cells, pushes myelopoiesis toward increased eosinophil production resulting in systemic eosinophil accumulation. Here, parallels can be drawn with allergic conditions in which $CD4^+$ T cells and eosinophils have a pathogenic function. In patients with allergic asthma, $CD4^+$ T cells play a major role in the pathophysiology driving eosinophil expansion via IL-5 production.[44,55] How ICB triggers this mechanism in the cancer context is not fully elucidated, but we demonstrated that $CD4^+$ T cells of TNBC patients upregulate IL-5 *in vivo* and *in vitro* upon stimulation with nivolumab/aPD-1, indicating that ICB can directly stimulate $CD4^+$ T cells to secrete IL-5. A role for PD-1/PD-L1 signaling in controlling IL-5 secretion from $CD4^+$ T cells has previously been proposed in the context of allergy, where *in vitro* exposure of human allergen-specific $CD4^+$ T cells to PD-1 blockade stimulated their production of IL-5, among other cytokines.[56] Altogether, we demonstrate that ICB-activated $CD4^+$ T cells use a similar mechanism via IL-5 to drive eosinophil accumulation in cancer patients and preclinical models.

Although neutrophils and basophils also derive from common myeloid progenitors, express IL5R and can respond to IL-5 in certain inflammatory conditions,[57,58] IL-5 is the central cytokine specific to eosinophil development in the bone marrow.[59] IL-33 is also implicated in eosinophil development, capable of inducing IL-5 and upregulating IL-5Rα on eosinophil progenitors.[60] Interestingly, we observe that ICB, in the absence of chemotherapy, increases IL-5 expression but not IL-33, indicating that ICB-induced IL-5 is not dependent on IL-33. This is further supported by our observation that systemic eosinophil abundance was unchanged upon IL-33 blockade during CIS + ICB, confirming that IL-5 is the main driver of eosinophil production in the bone marrow and systemic eosinophil accumulation upon ICB.

We demonstrate that ICB can be sufficient to induce systemic eosinophil increase, but in the majority of patients and in our mouse models (which do not respond to ICB alone), this is not enough to achieve intratumoral eosinophil infiltration. We uncover that induction of IL-33 is needed to overcome this threshold and enable eosinophil infiltration into the tumor. IL-33 can either directly affect eosinophil activation and recruitment, as has been shown for eosinophils in inflammatory diseases,[49,50] or indirectly by acting on other cells of the tumor microenvironment, for instance, by promoting chemokine expression in tumor cells.[16] IL-33 can be passively released by epithelial cells upon cellular damage[61] or actively secreted by immune cells during infection[62] and tumor cells themselves.[63] Importantly, in our mouse models cisplatin alone was not sufficient to increase IL-33 expression, indicating that cell damage induced by chemotherapy is not the sole driver of increased IL-33. By combining CIS + ICB we were able overcome this threshold and kick start the IL-33 aspect of the cascade in our mouse models. Future research is warranted to understand which other therapeutic modalities besides cisplatin may induce intratumoral IL-33 and whether these depend on cancer cell-intrinsic features or context-dependent mechanisms remains to be elucidated. For example, in patients, the net-biological effect of IL-33 is influenced by levels of soluble ST2 (also known as *IL1RL1*), which acts as a decoy receptor for IL-33, and for which different genetic variants exist in humans.[64] Thus, adding layers of complexity to the regulation of the identified immune axis. Identifying the source of IL-33 and deciphering how its production is regulated during ICB would be important to further harness its full therapeutic potential to synergize with ICB.

The synergy between rIL-33 and ICB has been studied in highly immunogenic models,[65,66] but not, to our knowledge, in poorly immunogenic breast cancer models. Our observation that IL-33 expression correlates with an eosinophil signature in metastases of breast cancer patients that respond to ICB and our preclinical proof-of-principle study demonstrating that rIL-33 mobilizes eosinophils to improve ICB response, indicate that IL-33 represents an attractive engager of eosinophils in breast cancer patients during ICB. However, IL-33 is reported to have pleiotropic functions.[67] The systemic administration of rIL-33, as performed in this study, induced an effective but modest anti-tumor response, especially in comparison with CIS + ICB, likely because of the direct anti-tumor effect and additional immunomodulatory properties of cisplatin.[68,69] Further studies are needed to evaluate whether IL-33 in combination with ICB could be used to specifically engage eosinophils in patients, for instance, by local IL-33 administration, although, in the context of multi-organ metastatic disease, local administration of rIL-33 would be challenging.

It has been suggested that ICB-induced eosinophils may exert direct tumoricidal effects or enhance anti-tumor immunity by changing the tumor vasculature or reshaping the immune landscape.[6] Eosinophils can facilitate recruitment of $CD8^+$ T cells by expression of T cell chemoattractants[11,25] or promote T cell activation in the tumor.[13] We demonstrate that eosinophils enhance $CD8^+$ T cell activation, rather than their recruitment, in mammary tumors responding to CIS + ICB. In line with our findings in mouse models, we observed that increased expression of an eosinophil gene signature correlated with increased $CD8^+$ T cell and IFN-γ gene signatures in metastatic lesions of breast cancer patients responding to ICB. This suggests that, in TNBC patients, eosinophils also contribute to ICB response via activation of $CD8^+$ T cells, as was previously proposed for melanoma patients.[19] It remains to be determined whether eosinophils exert this function directly, for example, by producing T cell-stimulating cytokines or chemokines, or indirectly via activation of, for instance, DCs, as has been described during allergic inflammation.[70–72]

In our study, the treatment of mice and patients differed. In our mouse models cisplatin and dual ICB was needed to induce responses, while patients were treated with ICB alone or preluded by a brief induction treatment. Despite these differences in dosage regime and type of ICB therapy, we strikingly uncovered the same phenomena of increased eosinophils in response to ICB, indicating that the mechanism described in this study is a general feature of effective ICB response. This is supported by

our observation that response to ICB leads to eosinophil accumulation in several cancer types and by a recent small series of 14 TNBC patients in which an eosinophil increase was observed upon response to anti-PD-L1 and paclitaxel.[73] In addition, we validated in patients the different elements of the mechanism identified in our preclinical models. We observed that circulating $CD4^+$ T cells of TNBC patients upregulate IL-5 expression upon nivolumab treatment *in vivo* and *in vitro*. Moreover, our data demonstrating that IL-5 is secreted in tumors that show an immunological response upon *ex vivo* ICB stimulation with either aPD-1 or combined aPD-1 + aCTLA-4, further strengthen our conclusion that IL-5 induction is a common mechanism across different tumor types and ICB regimens with or without chemotherapy.

Finally, it has been suggested that increased eosinophil counts upon ICB could be used as an early predictive biomarker for response.[19–24] Although we see expansion of these cells upon response to ICB in patients with metastatic TNBC, NSCLC, and early-stage pMMR CC, on-treatment response biomarkers are rarely used in oncology due to widely available imaging methods for response assessment. Moreover, eosinophil expansion was not restricted to responders, but was also observed in a proportion of non-responders as previously reported, limiting its potential for clinical decision making.[19–24] Therefore, increased eosinophils upon ICB response, combined with our preclinical proof of their causal role in ICB response, should be considered as an important lead for the development of immunomodulatory strategies to engage eosinophils rather than a biomarker.

In conclusion, this study highlights that combining translational research on clinical trials with mechanistic research in preclinical models is a powerful strategy to unravel mechanisms of ICB response. Our findings emphasize that successful anti-tumor immune responses are not only reliant on T cells, but that crosstalk with myeloid cells is critical for an effective response to ICB, providing avenues for future research in immuno-oncology.

STAR★METHODS

Detailed methods are provided in the online version of this paper and include the following:

- KEY RESOURCES TABLE
- RESOURCE AVAILABILITY
  - Lead contact
  - Materials availability
  - Data and code availability
- EXPERIMENTAL MODEL AND SUBJECT DETAILS
  - Preclinical models
  - Clinical trial procedures
- METHOD DETAILS
  - Preclinical intervention studies
  - Flow cytometry analysis
  - Immunohistochemistry
  - RNA-sequencing of mouse eosinophils
  - Cytokine analysis
  - Routine eosinophil counts in patient cohorts
  - RNA extraction and NanoString gene expression analysis
  - RNA-sequencing on patient tumor biopsies
  - RT-qPCR
  - Human PBMC stimulation
  - PDTF culture and stimulation
- QUANTIFICATIONS AND STATISTICAL ANALYSIS
- ADDITIONAL RESOURCES

SUPPLEMENTAL INFORMATION

Supplemental information can be found online at https://doi.org/10.1016/j.ccell.2022.11.014.

ACKNOWLEDGMENTS

We thank the patients and their families for participating in the clinical studies. We thank the Dutch Cancer Society (KWF10083 and KWF13191) and the Swiss National Science Foundation (P2FRP3_171794 and P400PM_18318/1 to L.S.) for funding the preclinical studies. We thank the BMS-International Immuno-Oncology Network (BMS/II-ON) and the Dutch Cancer Society (NKI2015-7710) for funding the TONIC study. The Dutch Cancer Society (10653ALPE) and A Sister's Hope contributed to the immunophenotyping of the TNBC patients. Research in the Kok group is funded by the Netherlands Organisation for Scientific Research (NWO-VIDI 09150172010043) and the Hendrika Roet fund. Research in the de Visser laboratory is funded by the Dutch Cancer Society (KWF10623), Oncode Institute, KWF/Oncode grant 14339, and the Netherlands Organisation for Scientific Research (NWO-VICI91819616). This research was further supported by an institutional grant to the NKI of the Dutch Cancer Society and the Dutch Ministry of Health, Welfare and Sport. I.S.A. holds a fundamental mandate of the Foundation against Cancer. We acknowledge the supporting staff of the clinical trials of the Departments of Medical Oncology, Biometrics, Clinical Chemistry and the Trialab. We acknowledge the Core Facility of Molecular Pathology & Biobanking and Michiel de Maaker for human RNA isolations and the Genomics Core Facility for RNA sequencing support. We thank the Animal Laboratory Facility, Intervention Unit, Imaging Unit, Experimental Animal Pathology Facility, and Flow Cytometry Facility for their support. Finally, we would like to thank everyone in the de Visser and Kok labs for inspiring discussions.

AUTHOR CONTRIBUTIONS

O.S.B., H.G., L.S., L.V., K.E.d.V., and M.K. designed and performed experiments, analyzed and interpreted the data, and wrote the manuscript. O.S.B. and L.S. performed the preclinical experiments with contributions from K. Kersten, H.G., D.P., C.-S.H., K.V., E.A.M.R., D.K., K. Kos, I.S.A., and R.B., supervised by K.E.d.V. H.G. performed the blood phenotyping of the TONIC trial together with N.B., C.K., M.D., M.B., and K.V., supervised by K.E.d.V. and M.K. L.V. coordinated and analyzed the data of the TONIC trial of which M.K. is the principal investigator. O.I.I. and E.v.D. performed bioinformatic analysis on the RNA sequencing and blood phenotyping data of the TONIC trial, respectively. M.C., W.S.M.E.T., and L.H. coordinated trial procedures and collected clinical data of the NICHE, PEMBRO-RT, and DRUP trials, respectively. P.B. and E.E.V. are the principal investigators of the PEMBRO-RT and DRUP trials, respectively. P.K. and D.S.T. developed and analyzed the data of the PDTF platform. L.F.A.W. supervised bioinformatic and statistical analysis and contributed to interpreting the results. All authors edited and approved the manuscript.

DECLARATION OF INTERESTS

O.S.B., H.G., L.S., L.V., O.I.I., E.v.D., N.B., C.K., M.D., K. Kersten, M.B., D.P., C.-S.H., K.V., E.A.M.R., D.K., L.H., K. Kos, I.S.A., P.K., R.B., and D.S.T. have no competing interests to declare. M.C. reports funding to the institute from BMS and Roche/Genentech and an advisory role for BMS, outside the submitted work. W.S.M.E.T. reports receiving grants from MSD during the conduct of the PEMBRO-RT trial. P.B. reports receiving grants and medication delivery from MSD during the conduct of the PEMBRO-RT trial as well as grants and consultancy fees from BMS outside the submitted work. E.E.V. is legally

responsible for all contracts with pharmaceutical companies at the NKI and reports research funding from BMS, outside the submitted work. L.F.A.W. reports funding to the institute from Genmab BV. K.E.d.V. reports research funding from Roche/Genentech and is consultant for Macomics, outside the scope of this work. M.K. reports funding to the institute from BMS, Roche/Genentech, AZ, and an advisory role for BMS, Roche, MSD, and Daiichi Sankyo, outside the submitted work.

Received: March 1, 2022
Revised: September 30, 2022
Accepted: November 23, 2022
Published: December 15, 2022

REFERENCES

1. Adams, S., Schmid, P., Rugo, H.S., Winer, E.P., Loirat, D., Awada, A., Cescon, D.W., Iwata, H., Campone, M., Nanda, R., et al. (2019). Pembrolizumab monotherapy for previously treated metastatic triple-negative breast cancer: cohort A of the phase II KEYNOTE-086 study. Ann. Oncol. *30*, 397–404. https://doi.org/10.1093/annonc/mdy517.
2. Winer, E.P., Lipatov, O., Im, S.A., Goncalves, A., Muñoz-Couselo, E., Lee, K.S., Schmid, P., Tamura, K., Testa, L., Witzel, I., et al. (2021). Pembrolizumab versus investigator-choice chemotherapy for metastatic triple-negative breast cancer (KEYNOTE-119): a randomised, open-label, phase 3 trial. Lancet Oncol. *22*, 499–511. https://doi.org/10.1016/s1470-2045(20)30754-3.
3. Schmid, P., Rugo, H.S., Adams, S., Schneeweiss, A., Barrios, C.H., Iwata, H., Diéras, V., Henschel, V., Molinero, L., Chui, S.Y., et al. (2020). Atezolizumab plus nab-paclitaxel as first-line treatment for unresectable, locally advanced or metastatic triple-negative breast cancer (IMpassion130): updated efficacy results from a randomised, double-blind, placebo-controlled, phase 3 trial. Lancet Oncol. *21*, 44–59. https://doi.org/10.1016/S1470-2045(19)30689-8.
4. Cortes, J., Cescon, D.W., Rugo, H.S., Nowecki, Z., Im, S.A., Yusof, M.M., Gallardo, C., Lipatov, O., Barrios, C.H., Holgado, E., et al. (2020). Pembrolizumab plus chemotherapy versus placebo plus chemotherapy for previously untreated locally recurrent inoperable or metastatic triple-negative breast cancer (KEYNOTE-355): a randomised, placebo-controlled, double-blind, phase 3 clinical trial. Lancet *396*, 1817–1828. https://doi.org/10.1016/s0140-6736(20)32531-9.
5. Demaria, O., Cornen, S., Daëron, M., Morel, Y., Medzhitov, R., and Vivier, E. (2019). Harnessing innate immunity in cancer therapy. Nature *574*, 45–56. https://doi.org/10.1038/s41586-019-1593-5.
6. Grisaru-Tal, S., Itan, M., Klion, A.D., and Munitz, A. (2020). A new dawn for eosinophils in the tumour microenvironment. Nat. Rev. Cancer *20*, 594–607. https://doi.org/10.1038/s41568-020-0283-9.
7. Grisaru-Tal, S., Rothenberg, M.E., and Munitz, A. (2022). Eosinophil-lymphocyte interactions in the tumor microenvironment and cancer immunotherapy. Nat. Immunol. *23*, 1309–1316. https://doi.org/10.1038/s41590-022-01291-2.
8. Rosenberg, H.F., Dyer, K.D., and Foster, P.S. (2013). Eosinophils: changing perspectives in health and disease. Nat. Rev. Immunol. *13*, 9–22. https://doi.org/10.1038/nri3341.
9. Kratochvill, F., Neale, G., Haverkamp, J.M., Van de Velde, L.A., Smith, A.M., Kawauchi, D., McEvoy, J., Roussel, M.F., Dyer, M.A., Qualls, J.E., and Murray, P.J. (2015). TNF counterbalances the emergence of M2 tumor macrophages. Cell Rep. *12*, 1902–1914. https://doi.org/10.1016/j.celrep.2015.08.033.
10. Zaynagetdinov, R., Sherrill, T.P., Gleaves, L.A., McLoed, A.G., Saxon, J.A., Habermann, A.C., Connelly, L., Dulek, D., Peebles, R.S., Jr., Fingleton, B., et al. (2015). Interleukin-5 facilitates lung metastasis by modulating the immune microenvironment. Cancer Res. *75*, 1624–1634. https://doi.org/10.1158/0008-5472.can-14-2379.
11. Carretero, R., Sektioglu, I.M., Garbi, N., Salgado, O.C., Beckhove, P., and Hämmerling, G.J. (2015). Eosinophils orchestrate cancer rejection by normalizing tumor vessels and enhancing infiltration of CD8(+) T cells. Nat. Immunol. *16*, 609–617. https://doi.org/10.1038/ni.3159.
12. Jia, S., Li, W., Liu, P., and Xu, L.X. (2019). A role of eosinophils in mediating the anti-tumour effect of cryo-thermal treatment. Sci. Rep. *9*, 13214. https://doi.org/10.1038/s41598-019-49734-5.
13. Arnold, I.C., Artola-Boran, M., Gurtner, A., Bertram, K., Bauer, M., Frangez, Z., Becher, B., Kopf, M., Yousefi, S., Simon, H.U., et al. (2020). The GM-CSF-IRF5 signaling axis in eosinophils promotes antitumor immunity through activation of type 1 T cell responses. J. Exp. Med. *217*, e20190706. https://doi.org/10.1084/jem.20190706.
14. Hollande, C., Boussier, J., Ziai, J., Nozawa, T., Bondet, V., Phung, W., Lu, B., Duffy, D., Paradis, V., Mallet, V., et al. (2019). Inhibition of the dipeptidyl peptidase DPP4 (CD26) reveals IL-33-dependent eosinophil-mediated control of tumor growth. Nat. Immunol. *20*, 257–264. https://doi.org/10.1038/s41590-019-0321-5.
15. Reichman, H., Itan, M., Rozenberg, P., Yarmolovski, T., Brazowski, E., Varol, C., Gluck, N., Shapira, S., Arber, N., Qimron, U., et al. (2019). Activated eosinophils exert antitumorigenic activities in colorectal cancer. Cancer Immunol. Res. *7*, 388–400. https://doi.org/10.1158/2326-6066.CIR-18-0494.
16. Andreone, S., Spadaro, F., Buccione, C., Mancini, J., Tinari, A., Sestili, P., Gambardella, A.R., Lucarini, V., Ziccheddu, G., Parolini, I., et al. (2019). IL-33 promotes CD11b/CD18-mediated adhesion of eosinophils to cancer cells and synapse-polarized degranulation leading to tumor cell killing. Cancers *11*, 1664. https://doi.org/10.3390/cancers11111664.
17. Varricchi, G., Galdiero, M.R., Loffredo, S., Lucarini, V., Marone, G., Mattei, F., Marone, G., and Schiavoni, G. (2018). Eosinophils: the unsung heroes in cancer? OncoImmunology *7*, e1393134. https://doi.org/10.1080/2162402x.2017.1393134.
18. Grisaru-Tal, S., Dulberg, S., Beck, L., Zhang, C., Itan, M., Hediyeh-Zadeh, S., Caldwell, J., Rozenberg, P., Dolitzky, A., Avlas, S., et al. (2021). Metastasis-entrained eosinophils enhance lymphocyte-mediated antitumor immunity. Cancer Res. *81*, 5555–5571. https://doi.org/10.1158/0008-5472.can-21-0839.
19. Simon, S.C.S., Hu, X., Panten, J., Grees, M., Renders, S., Thomas, D., Weber, R., Schulze, T.J., Utikal, J., and Umansky, V. (2020). Eosinophil accumulation predicts response to melanoma treatment with immune checkpoint inhibitors. OncoImmunology *9*, 1727116. https://doi.org/10.1080/2162402X.2020.1727116.
20. Delyon, J., Mateus, C., Lefeuvre, D., Lanoy, E., Zitvogel, L., Chaput, N., Roy, S., Eggermont, A.M.M., Routier, E., and Robert, C. (2013). Experience in daily practice with ipilimumab for the treatment of patients with metastatic melanoma: an early increase in lymphocyte and eosinophil counts is associated with improved survival. Ann. Oncol. *24*, 1697–1703. https://doi.org/10.1093/annonc/mdt027.
21. Gebhardt, C., Sevko, A., Jiang, H., Lichtenberger, R., Reith, M., Tarnanidis, K., Holland-Letz, T., Umansky, L., Beckhove, P., Sucker, A., et al. (2015). Myeloid cells and related chronic inflammatory factors as novel predictive markers in melanoma treatment with ipilimumab. Clin. Cancer Res. *21*, 5453–5459. https://doi.org/10.1158/1078-0432.Ccr-15-0676.
22. Alves, A., Dias, M., Campainha, S., and Barroso, A. (2021). Peripheral blood eosinophilia may be a prognostic biomarker in non-small cell lung cancer patients treated with immunotherapy. J. Thorac. Dis. *13*, 2716–2727. https://doi.org/10.21037/jtd-20-3525.
23. Okauchi, S., Shiozawa, T., Miyazaki, K., Nishino, K., Sasatani, Y., Ohara, G., Kagohashi, K., Sato, S., Kodama, T., Satoh, H., and Hizawa, N. (2021). Association between peripheral eosinophils and clinical outcomes in patients with non-small cell lung cancer treated with immune checkpoint inhibitors. Pol. Arch. Intern. Med. *131*, 152–160. https://doi.org/10.20452/pamw.15776.
24. Verhaart, S.L., Abu-Ghanem, Y., Mulder, S.F., Oosting, S., Van Der Veldt, A., Osanto, S., Aarts, M.J.B., Houtsma, D., Peters, F.P.J., Groenewegen, G., et al. (2021). Real-world data of nivolumab for patients with advanced renal cell carcinoma in The Netherlands: an analysis of toxicity, efficacy,

and predictive markers. Clin. Genitourin. Cancer *19*, 274.e1–274.e16. https://doi.org/10.1016/j.clgc.2020.10.003.

25. Zheng, X., Zhang, N., Qian, L., Wang, X., Fan, P., Kuai, J., Lin, S., Liu, C., Jiang, W., Qin, S., et al. (2020). CTLA4 blockade promotes vessel normalization in breast tumors via the accumulation of eosinophils. Int. J. Cancer *146*, 1730–1740. https://doi.org/10.1002/ijc.32829.
26. Coffelt, S.B., Kersten, K., Doornebal, C.W., Weiden, J., Vrijland, K., Hau, C.S., Verstegen, N.J.M., Ciampricotti, M., Hawinkels, L.J.A.C., Jonkers, J., and de Visser, K.E. (2015). IL-17-producing γδ T cells and neutrophils conspire to promote breast cancer metastasis. Nature *522*, 345–348. https://doi.org/10.1038/nature14282.
27. Salvagno, C., Ciampricotti, M., Tuit, S., Hau, C.S., van Weverwijk, A., Coffelt, S.B., Kersten, K., Vrijland, K., Kos, K., Ulas, T., et al. (2019). Therapeutic targeting of macrophages enhances chemotherapy efficacy by unleashing type I interferon response. Nat. Cell Biol. *21*, 511–521. https://doi.org/10.1038/s41556-019-0298-1.
28. Voorwerk, L., Slagter, M., Horlings, H.M., Sikorska, K., van de Vijver, K.K., de Maaker, M., Nederlof, I., Kluin, R.J.C., Warren, S., Ong, S., et al. (2019). Immune induction strategies in metastatic triple-negative breast cancer to enhance the sensitivity to PD-1 blockade: the TONIC trial. Nat. Med. *25*, 920–928. https://doi.org/10.1038/s41591-019-0432-4.
29. Theelen, W.S.M.E., Peulen, H.M.U., Lalezari, F., van der Noort, V., de Vries, J.F., Aerts, J.G.J.V., Dumoulin, D.W., Bahce, I., Niemeijer, A.L.N., de Langen, A.J., et al. (2019). Effect of pembrolizumab after stereotactic body radiotherapy vs pembrolizumab alone on tumor response in patients with advanced non-small cell lung cancer: results of the PEMBRO-RT phase 2 randomized clinical trial. JAMA Oncol. *5*, 1276–1282. https://doi.org/10.1001/jamaoncol.2019.1478.
30. Chalabi, M., Fanchi, L.F., Dijkstra, K.K., Van den Berg, J.G., Aalbers, A.G., Sikorska, K., Lopez-Yurda, M., Grootscholten, C., Beets, G.L., Snaebjornsson, P., et al. (2020). Neoadjuvant immunotherapy leads to pathological responses in MMR-proficient and MMR-deficient early-stage colon cancers. Nat. Med. *26*, 566–576. https://doi.org/10.1038/s41591-020-0805-8.
31. van der Velden, D.L., Hoes, L.R., van der Wijngaart, H., van Berge Henegouwen, J.M., van Werkhoven, E., Roepman, P., Schilsky, R.L., de Leng, W.W.J., Huitema, A.D.R., Nuijen, B., et al. (2019). The Drug Rediscovery protocol facilitates the expanded use of existing anticancer drugs. Nature *574*, 127–131. https://doi.org/10.1038/s41586-019-1600-x.
32. Kikly, K.K., Bochner, B.S., Freeman, S.D., Tan, K.B., Gallagher, K.T., D'alessio, K.J., Holmes, S.D., Abrahamson, J.A., Erickson-Miller, C.L., Murdock, P.R., et al. (2000). Identification of SAF-2, a novel siglec expressed on eosinophils, mast cells, and basophils. J. Allergy Clin. Immunol. *105*, 1093–1100. https://doi.org/10.1067/mai.2000.107127.
33. Ayers, M., Lunceford, J., Nebozhyn, M., Murphy, E., Loboda, A., Kaufman, D.R., Albright, A., Cheng, J.D., Kang, S.P., Shankaran, V., et al. (2017). IFN-gamma-related mRNA profile predicts clinical response to PD-1 blockade. J. Clin. Invest. *127*, 2930–2940. https://doi.org/10.1172/jci91190.
34. Derksen, P.W.B., Liu, X., Saridin, F., van der Gulden, H., Zevenhoven, J., Evers, B., van Beijnum, J.R., Griffioen, A.W., Vink, J., Krimpenfort, P., et al. (2006). Somatic inactivation of E-cadherin and p53 in mice leads to metastatic lobular mammary carcinoma through induction of anoikis resistance and angiogenesis. Cancer Cell *10*, 437–449. https://doi.org/10.1016/j.ccr.2006.09.013.
35. Doornebal, C.W., Klarenbeek, S., Braumuller, T.M., Klijn, C.N., Ciampricotti, M., Hau, C.S., Hollmann, M.W., Jonkers, J., and de Visser, K.E. (2013). A preclinical mouse model of invasive lobular breast cancer metastasis. Cancer Res. *73*, 353–363. https://doi.org/10.1158/0008-5472.Can-11-4208.
36. Beyranvand Nejad, E., van der Sluis, T.C., van Duikeren, S., Yagita, H., Janssen, G.M., van Veelen, P.A., Melief, C.J.M., van der Burg, S.H., and Arens, R. (2016). Tumor eradication by cisplatin is sustained by CD80/86-mediated costimulation of CD8+ T cells. Cancer Res. *76*, 6017–6029. https://doi.org/10.1158/0008-5472.CAN-16-0881.
37. Nolan, E., Savas, P., Policheni, A.N., Darcy, P.K., Vaillant, F., Mintoff, C.P., Dushyanthen, S., Mansour, M., Pang, J.M.B., Fox, S.B., et al. (2017). Combined immune checkpoint blockade as a therapeutic strategy for BRCA1-mutated breast cancer. Sci. Transl. Med. *9*, eaal4922. https://doi.org/10.1126/scitranslmed.aal4922.
38. Grimaldi, A., Cammarata, I., Martire, C., Focaccetti, C., Piconese, S., Buccilli, M., Mancone, C., Buzzacchino, F., Berrios, J.R.G., D'Alessandris, N., et al. (2020). Combination of chemotherapy and PD-1 blockade induces T cell responses to tumor non-mutated neoantigens. Commun. Biol. *3*, 85. https://doi.org/10.1038/s42003-020-0811-x.
39. Wan, S., Pestka, S., Jubin, R.G., Lyu, Y.L., Tsai, Y.C., and Liu, L.F. (2012). Chemotherapeutics and radiation stimulate MHC class I expression through elevated interferon-beta signaling in breast cancer cells. PLoS One *7*, e32542. https://doi.org/10.1371/journal.pone.0032542.
40. Cheng, J.N., Luo, W., Sun, C., Jin, Z., Zeng, X., Alexander, P.B., Gong, Z., Xia, X., Ding, X., Xu, S., et al. (2021). Radiation-induced eosinophils improve cytotoxic T lymphocyte recruitment and response to immunotherapy. Sci. Adv. *7*, eabc7609. https://doi.org/10.1126/sciadv.abc7609.
41. Zimmermann, N., McBride, M.L., Yamada, Y., Hudson, S.A., Jones, C., Cromie, K.D., Crocker, P.R., Rothenberg, M.E., and Bochner, B.S. (2008). Siglec-F antibody administration to mice selectively reduces blood and tissue eosinophils. Allergy *63*, 1156–1163. https://doi.org/10.1111/j.1398-9995.2008.01709.x.
42. Pfirschke, C., Engblom, C., Gungabeesoon, J., Lin, Y., Rickelt, S., Zilionis, R., Messemaker, M., Siwicki, M., Gerhard, G.M., Kohl, A., et al. (2020). Tumor-promoting Ly-6G(+) SiglecF(high) cells are mature and long-lived neutrophils. Cell Rep. *32*, 108164. https://doi.org/10.1016/j.celrep.2020.108164.
43. Iwasaki, H., Mizuno, S.i., Mayfield, R., Shigematsu, H., Arinobu, Y., Seed, B., Gurish, M.F., Takatsu, K., and Akashi, K. (2005). Identification of eosinophil lineage-committed progenitors in the murine bone marrow. J. Exp. Med. *201*, 1891–1897. https://doi.org/10.1084/jem.20050548.
44. Pelaia, C., Paoletti, G., Puggioni, F., Racca, F., Pelaia, G., Canonica, G.W., and Heffler, E. (2019). Interleukin-5 in the pathophysiology of severe asthma. Front. Physiol. *10*, 1514. https://doi.org/10.3389/fphys.2019.01514.
45. Voabil, P., de Bruijn, M., Roelofsen, L.M., Hendriks, S.H., Brokamp, S., van den Braber, M., Broeks, A., Sanders, J., Herzig, P., Zippelius, A., et al. (2021). An ex vivo tumor fragment platform to dissect response to PD-1 blockade in cancer. Nat. Med. *27*, 1250–1261. https://doi.org/10.1038/s41591-021-01398-3.
46. Kaptein, P., Jacoberger-Foissac, C., Dimitriadis, P., Voabil, P., de Bruijn, M., Brokamp, S., Reijers, I., Versluis, J., Nallan, G., Triscott, H., et al. (2022). Addition of interleukin-2 overcomes resistance to neoadjuvant CTLA4 and PD1 blockade in ex vivo patient tumors. Sci. Transl. Med. *14*, eabj9779. https://doi.org/10.1126/scitranslmed.abj9779.
47. Kos, K., Aslam, M.A., van de Ven, R., Wellenstein, M.D., Pieters, W., van Weverwijk, A., Duits, D.E.M., van Pul, K., Hau, C.S., Vrijland, K., et al. (2022). Tumor-educated T(regs) drive organ-specific metastasis in breast cancer by impairing NK cells in the lymph node niche. Cell Rep. *38*, 110447. https://doi.org/10.1016/j.celrep.2022.110447.
48. Chan, B.C.L., Lam, C.W.K., Tam, L.S., and Wong, C.K. (2019). IL33: roles in allergic inflammation and therapeutic perspectives. Front. Immunol. *10*, 364. https://doi.org/10.3389/fimmu.2019.00364.
49. Cherry, W.B., Yoon, J., Bartemes, K.R., Iijima, K., and Kita, H. (2008). A novel IL-1 family cytokine, IL-33, potently activates human eosinophils. J. Allergy Clin. Immunol. *121*, 1484–1490. https://doi.org/10.1016/j.jaci.2008.04.005.
50. Suzukawa, M., Koketsu, R., Iikura, M., Nakae, S., Matsumoto, K., Nagase, H., Saito, H., Matsushima, K., Ohta, K., Yamamoto, K., and Yamaguchi, M. (2008). Interleukin-33 enhances adhesion, CD11b expression and survival in human eosinophils. Lab. Invest. *88*, 1245–1253. https://doi.org/10.1038/labinvest.2008.82.

51. Johnston, L.K., and Bryce, P.J. (2017). Understanding interleukin 33 and its roles in eosinophil development. Front. Med. *4*, 51. https://doi.org/10.3389/fmed.2017.00051.

52. Shani, O., Vorobyov, T., Monteran, L., Lavie, D., Cohen, N., Raz, Y., Tsarfaty, G., Avivi, C., Barshack, I., and Erez, N. (2020). Fibroblast-derived IL33 facilitates breast cancer metastasis by modifying the immune microenvironment and driving type 2 immunity. Cancer Res. *80*, 5317–5329. https://doi.org/10.1158/0008-5472.can-20-2116.

53. Lucarini, V., Zicchedda, G., Macchia, I., La Sorsa, V., Peschiaroli, F., Buccione, C., Sistigu, A., Sanchez, M., Andreone, S., D'Urso, M.T., et al. (2017). IL-33 restricts tumor growth and inhibits pulmonary metastasis in melanoma-bearing mice through eosinophils. OncoImmunology *6*, e1317420. https://doi.org/10.1080/2162402X.2017.1317420.

54. Holgado, A., Braun, H., Van Nuffel, E., Detry, S., Schuijs, M.J., Deswarte, K., Vergote, K., Haegman, M., Baudelet, G., Haustraete, J., et al. (2019). IL-33trap is a novel IL-33-neutralizing biologic that inhibits allergic airway inflammation. J. Allergy Clin. Immunol. *144*, 204–215. https://doi.org/10.1016/j.jaci.2019.02.028.

55. Ling, M.F., and Luster, A.D. (2016). Allergen-specific CD4(+) T cells in human asthma. Ann. Am. Thorac. Soc. *13*, S25–S30. https://doi.org/10.1513/AnnalsATS.201507-431MG.

56. Rosskopf, S., Jahn-Schmid, B., Schmetterer, K.G., Zlabinger, G.J., and Steinberger, P. (2018). PD-1 has a unique capacity to inhibit allergen-specific human CD4(+) T cell responses. Sci. Rep. *8*, 13543. https://doi.org/10.1038/s41598-018-31757-z.

57. Gorski, S.A., Lawrence, M.G., Hinkelman, A., Spano, M.M., Steinke, J.W., Borish, L., Teague, W.G., and Braciale, T.J. (2019). Expression of IL-5 receptor alpha by murine and human lung neutrophils. PLoS One *14*, e0221113. https://doi.org/10.1371/journal.pone.0221113.

58. Kolbeck, R., Kozhich, A., Koike, M., Peng, L., Andersson, C.K., Damschroder, M.M., Reed, J.L., Woods, R., Dall'acqua, W.W., Stephens, G.L., et al. (2010). MEDI-563, a humanized anti-IL-5 receptor alpha mAb with enhanced antibody-dependent cell-mediated cytotoxicity function. J. Allergy Clin. Immunol. *125*, 1344–1353.e2. https://doi.org/10.1016/j.jaci.2010.04.004.

59. Dent, L.A., Strath, M., Mellor, A.L., and Sanderson, C.J. (1990). Eosinophilia in transgenic mice expressing interleukin 5. J. Exp. Med. *172*, 1425–1431. https://doi.org/10.1084/jem.172.5.1425.

60. Johnston, L.K., Hsu, C.L., Krier-Burris, R.A., Chhiba, K.D., Chien, K.B., McKenzie, A., Berdnikovs, S., and Bryce, P.J. (2016). IL-33 precedes IL-5 in regulating eosinophil commitment and is required for eosinophil homeostasis. J. Immunol. *197*, 3445–3453. https://doi.org/10.4049/jimmunol.1600611.

61. Pichery, M., Mirey, E., Mercier, P., Lefrancais, E., Dujardin, A., Ortega, N., and Girard, J.P. (2012). Endogenous IL-33 is highly expressed in mouse epithelial barrier tissues, lymphoid organs, brain, embryos, and inflamed tissues: in situ analysis using a novel Il-33-LacZ gene trap reporter strain. J. Immunol. *188*, 3488–3495. https://doi.org/10.4049/jimmunol.1101977.

62. Hung, L.Y., Tanaka, Y., Herbine, K., Pastore, C., Singh, B., Ferguson, A., Vora, N., Douglas, B., Zullo, K., Behrens, E.M., et al. (2020). Cellular context of IL-33 expression dictates impact on anti-helminth immunity. Sci. Immunol. *5*, eabc6259. https://doi.org/10.1126/sciimmunol.abc6259.

63. Taniguchi, S., Elhance, A., Duzer, A.V., Kumar, S., Leitenberger, J.J., and Oshimori, N. (2020). Tumor-initiating cells establish an IL-33–TGF-β niche signaling loop to promote cancer progression. Science *369*, eaay1813. https://doi.org/10.1126/science.aay1813.

64. Saikumar Jayalatha, A.K., Hesse, L., Ketelaar, M.E., Koppelman, G.H., and Nawijn, M.C. (2021). The central role of IL-33/IL-1RL1 pathway in asthma: from pathogenesis to intervention. Pharmacol. Ther. *225*, 107847. https://doi.org/10.1016/j.pharmthera.2021.107847.

65. Jacquelot, N., Seillet, C., Wang, M., Pizzolla, A., Liao, Y., Hediyeh-Zadeh, S., Grisaru-Tal, S., Louis, C., Huang, Q., Schreuder, J., et al. (2021). Blockade of the co-inhibitory molecule PD-1 unleashes ILC2-dependent antitumor immunity in melanoma. Nat. Immunol. *22*, 851–864. https://doi.org/10.1038/s41590-021-00943-z.

66. Chen, L., Sun, R., Xu, J., Zhai, W., Zhang, D., Yang, M., Yue, C., Chen, Y., Li, S., Turnquist, H., et al. (2020). Tumor-derived IL33 promotes tissue-resident CD8(+) T cells and is required for checkpoint blockade tumor immunotherapy. Cancer Immunol. Res. *8*, 1381–1392. https://doi.org/10.1158/2326-6066.cir-19-1024.

67. Shen, J.X., Liu, J., and Zhang, G.J. (2018). Interleukin-33 in malignancies: friends or foes? Front. Immunol. *9*, 3051. https://doi.org/10.3389/fimmu.2018.03051.

68. Dasari, S., and Tchounwou, P.B. (2014). Cisplatin in cancer therapy: molecular mechanisms of action. Eur. J. Pharmacol. *740*, 364–378. https://doi.org/10.1016/j.ejphar.2014.07.025.

69. de Biasi, A.R., Villena-Vargas, J., and Adusumilli, P.S. (2014). Cisplatin-induced antitumor immunomodulation: a review of preclinical and clinical evidence. Clin. Cancer Res. *20*, 5384–5391. https://doi.org/10.1158/1078-0432.CCR-14-1298.

70. Jacobsen, E.A., Zellner, K.R., Colbert, D., Lee, N.A., and Lee, J.J. (2011). Eosinophils regulate dendritic cells and Th2 pulmonary immune responses following allergen provocation. J. Immunol. *187*, 6059–6068. https://doi.org/10.4049/jimmunol.1102299.

71. Kanda, A., Fleury, S., Kobayashi, Y., Tomoda, K., Julia, V., and Dombrowicz, D. (2015). Th2-activated eosinophils release Th1 cytokines that modulate allergic inflammation. Allergol. Int. *64*, S71–S73. https://doi.org/10.1016/j.alit.2015.03.006.

72. Jacobsen, E.A., Ochkur, S.I., Pero, R.S., Taranova, A.G., Protheroe, C.A., Colbert, D.C., Lee, N.A., and Lee, J.J. (2008). Allergic pulmonary inflammation in mice is dependent on eosinophil-induced recruitment of effector T cells. J. Exp. Med. *205*, 699–710. https://doi.org/10.1084/jem.20071840.

73. Ghebeh, H., Elshenawy, M.A., AlSayed, A.D., and Al-Tweigeri, T. (2022). Peripheral blood eosinophil count is associated with response to chemoimmunotherapy in metastatic triple-negative breast cancer. Immunotherapy *14*, 189–199. https://doi.org/10.2217/imt-2021-0149.

74. de Visser, K.E., Korets, L.V., and Coussens, L.M. (2005). De novo carcinogenesis promoted by chronic inflammation is B lymphocyte dependent. Cancer Cell *7*, 411–423. https://doi.org/10.1016/j.ccr.2005.04.014.

75. Kim, J.M., Rasmussen, J.P., and Rudensky, A.Y. (2007). Regulatory T cells prevent catastrophic autoimmunity throughout the lifespan of mice. Nat. Immunol. *8*, 191–197. https://doi.org/10.1038/ni1428.

76. Eisenhauer, E.A., Therasse, P., Bogaerts, J., Schwartz, L.H., Sargent, D., Ford, R., Dancey, J., Arbuck, S., Gwyther, S., Mooney, M., et al. (2009). New response evaluation criteria in solid tumours: revised RECIST guideline (version 1.1). Eur. J. Cancer *45*, 228–247. https://doi.org/10.1016/j.ejca.2008.10.026.

77. Seymour, L., Bogaerts, J., Perrone, A., Ford, R., Schwartz, L.H., Mandrekar, S., Lin, N.U., Litière, S., Dancey, J., Chen, A., et al. (2017). iRECIST: guidelines for response criteria for use in trials testing immunotherapeutics. Lancet Oncol. *18*, e143–e152. https://doi.org/10.1016/S1470-2045(17)30074-8.

78. Picelli, S., Faridani, O.R., Björklund, A.K., Winberg, G., Sagasser, S., and Sandberg, R. (2014). Full-length RNA-seq from single cells using Smart-seq2. Nat. Protoc. *9*, 171–181. https://doi.org/10.1038/nprot.2014.006.

79. Dobin, A., Davis, C.A., Schlesinger, F., Drenkow, J., Zaleski, C., Jha, S., Batut, P., Chaisson, M., and Gingeras, T.R. (2013). STAR: ultrafast universal RNA-seq aligner. Bioinformatics *29*, 15–21. https://doi.org/10.1093/bioinformatics/bts635.

80. Love, M.I., Huber, W., and Anders, S. (2014). Moderated estimation of fold change and dispersion for RNA-seq data with DESeq2. Genome Biol. *15*, 550. https://doi.org/10.1186/s13059-014-0550-8.

81. Pandas, D.t. (2020). pandas-dev/pandas: Pandas. Zenodo. https://doi.org/10.5281/zenodo.3509134.

82. McKinney, W. (2010). Data structures for statistical computing in Python from proceedings of the 9th Python in science conference, pp. 56–61. https://doi.org/10.25080/Majora-92bf1922-00a.

83. Harris, C.R., Millman, K.J., van der Walt, S.J., Gommers, R., Virtanen, P., Cournapeau, D., Wieser, E., Taylor, J., Berg, S., Smith, N.J., et al. (2020). Array programming with NumPy. Nature *585*, 357–362. https://doi.org/10.1038/s41586-020-2649-2.

84. Hunter, J.D. (2007). Matplotlib: a 2D graphics environment. Comput. Sci. Eng. *9*, 90–95. https://doi.org/10.1109/MCSE.2007.55.

85. Waskom, M., Botvinnik, O., O'Kane, D., Hobson, P., Lukauskas, S., Gemperline, D.C., Augspurger, T., Halchenko, Y., Cole, J.B., Warmenhoven, J., et al. (2017). mwaskom/seaborn: v0.8.1. Zenodo. https://doi.org/10.5281/zenodo.883859.

86. Weber, M. (2020). statannot 0.2.2.

87. Tateno, H., Crocker, P.R., and Paulson, J.C. (2005). Mouse Siglec-F and human Siglec-8 are functionally convergent paralogs that are selectively expressed on eosinophils and recognize 6'-sulfo-sialyl Lewis X as a preferred glycan ligand. Glycobiology *15*, 1125–1135. https://doi.org/10.1093/glycob/cwi097.

88. Abu-Ghazaleh, R.I., Dunnette, S.L., Loegering, D.A., Checkel, J.L., Kita, H., Thomas, L.L., and Gleich, G.J. (1992). Eosinophil granule proteins in peripheral blood granulocytes. J. Leukoc. Biol. *52*, 611–618. https://doi.org/10.1002/jlb.52.6.611.

89. Mori, Y., Iwasaki, H., Kohno, K., Yoshimoto, G., Kikushige, Y., Okeda, A., Uike, N., Niiro, H., Takenaka, K., Nagafuji, K., et al. (2009). Identification of the human eosinophil lineage-committed progenitor: revision of phenotypic definition of the human common myeloid progenitor. J. Exp. Med. *206*, 183–193. https://doi.org/10.1084/jem.20081756.

90. Höchstetter, R., Dobos, G., Kimmig, D., Dulkys, Y., Kapp, A., and Elsner, J. (2000). The CC chemokine receptor 3 CCR3 is functionally expressed on eosinophils but not on neutrophils. Eur. J. Immunol. *30*, 2759–2764. https://doi.org/10.1002/1521-4141(200010)30:10<2759::AID-IMMU2759>3.0.CO;2-A.

91. Alcover, A., Alarcón, B., and Di Bartolo, V. (2018). Cell biology of T cell receptor expression and regulation. Annu. Rev. Immunol. *36*, 103–125. https://doi.org/10.1146/annurev-immunol-042617-053429.

92. Li, Y., Yin, Y., and Mariuzza, R.A. (2013). Structural and biophysical insights into the role of CD4 and CD8 in T cell activation. Front. Immunol. *4*, 206. https://doi.org/10.3389/fimmu.2013.00206.

93. Wickham, H. (2016). ggplot2: Elegant Graphics for Data Analysis (New York: Springer-Verlag). https://ggplot2.tidyverse.org.

94. Kassambara, ggpubr: 'ggplot2'Based Publication Ready Plots, 2020. https://github.com/kassambara/ggpubr

95. Slowikowski, ggrepel. *Automatically Position Non-Overlapping Text Labels with 'ggplot2'*, 2021. https://CRAN.R-project.org/package=ggrepel.

96. Wickham. (2007). *Reshaping Data with the {reshape} Package*. http://www.jstatsoft.org/v21/i12/.

97. Wickham, et al. (2022). *A Grammar of Data Manipulation*. https://CRAN.R-project.org/package=dplyr.

98. Henry, et al. (2020). In purrr: Functional Programming Tools https://CRAN.R-project.org/package=purrr.

99. Zhao, et al. (2021). *heatmap3: An Improved Heatmap Package*. https://CRAN.R-project.org/package=heatmap3.

100. Clarke, et al. *ggbeeswarm: Categorical Scatter (Violin Point) Plots*. https://CRAN.R-project.org/package=ggbeeswarm.

STAR★METHODS

KEY RESOURCES TABLE

REAGENT or RESOURCE	SOURCE	IDENTIFIER
Antibodies		
Rat IgG2a, k anti-PD-1 (clone RMP1-14)	BioXCell	Cat# BE0146; RRID: AB_10949053
Mouse IgG2b anti-CTLA-4 (clone 9D9)	BioXCell	Cat# BE0164; RRID: AB_10949609
Rat IgG2a anti-SiglecF (clone 238047)	R&D systems	Cat# MAB17061; RRID: AB_2286029
Rat IgG2b anti-CD8 (clone 2.43)	BioXCell	Cat# BE0061; RRID: AB_1125541
Rat IgG1, k anti-IL-5 (clone TRFK5)	BioXCell	Cat# BE0198; RRID: AB_10950522
Rat IgG2b, k anti-CD4 (clone GK1.5)	BioXCell	Cat# BE0003-1; RRID: AB_1107636
Rat IgG2a isotype control antibody (clone 2A3)	BioXCell	Cat# BE0089; RRID: AB_1107769
Rat IgG1, k isotype control antibody (clone HRPN)	BioXCell	Cat# BE0088; RRID: AB_1107775
anti-mouse CCR3, APC (clone J073E5)	BioLegend	Cat# 144511; RRID: AB_2565737
anti-mouse CCR3, FITC (clone J073E5)	BioLegend	Cat# 144509; RRID: AB_2561608
anti-mouse CD101, PE-Cy7 (clone Moushi101)	eBioscience/ThermoFisher	Cat# 25-1011-82; RRID: AB_2573378
anti-mouse CD103, APC (clone M290)	BD Biosciences	Cat# 562772; RRID: AB_2737784
anti-mouse CD115, BV711 (clone AFS98)	BioLegend	Cat# 135515; RRID: AB_2562679
anti-mouse CD11b, BV786 (clone M1/70)	BD Biosciences	Cat# 740861; RRID: AB_2740514
anti-mouse CD11b, BV421 (clone M1/70)	BioLegend	Cat# 101236; RRID: AB_11203704
anti-mouse CD11b, PE-Cy7 (clone M1/70)	BD Biosciences	Cat# 561098; RRID:AB_394491
anti-mouse CD11c, BUV737 (clone HL3)	BD Biosciences	Cat# 612797; RRID:AB_2870124
anti-mouse CD11c, PE (clone HL3)	BD Biosciences	Cat# 553802; RRID: AB_395061
anti-mouse CD125, BUV737 (clone T21)	BD Biosciences	Cat# 741888; RRID: AB_2871209
anti-mouse CD127, PE-Dazzle (clone A7R34)	BioLegend	Cat# 135032; RRID: AB_2564217
anti-mouse CD137, APC (clone 17B5)	BioLegend	Cat# 106110; RRID: AB_2564297
anti-mouse CD150, BV650 (clone TC15-12F12.2)	BioLegend	Cat# 115932; RRID: AB_2715765
anti-mouse CD16/32 (clone 2.4G2)	BD Biosciences	Cat# 553141; RRID: AB_394656
anti-mouse CD16/32, BUV395 (clone 2.4G2)	BD Biosciences	Cat# 740217; RRID: AB_2739965
anti-mouse CD19, APC-eFluor780 (clone eBio1D3)	eBioscience/ThermoFisher	Cat# 47-0193-82; RRID: AB_10853189
anti-mouse CD19, PerCP-Cy5.5 (clone 1D3/CD19)	BioLegend	Cat# 152406; RRID: AB_2629815
anti-mouse CD25, APC (clone PC61)	BioLegend	Cat# 102011; RRID: AB_312860
anti-mouse CD25, PE (clone PC61)	BioLegend	Cat# 102008; RRID: AB_312857
anti-mouse CD34, AF647 (clone RAM34)	BD Biosciences	Cat# 560230; RRID: AB_1645200
anti-mouse CD3e, APC-eFluor780 (clone 500A2)	eBioscience/ThermoFisher	Cat# 47-0033-82; RRID: AB_2637316
anti-mouse CD3e, BV421 (clone 145-2C11)	BioLegend	Cat# 100335; RRID: AB_10898314
anti-mouse CD3e, PE-Cy7 (clone 145-2C11)	eBioscience/ThermoFisher	Cat# 25-0031-82; RRID: AB_469572
anti-mouse CD3e, PerCP-Cy5.5 (clone 145-2C11)	BD Biosciences	Cat# 551163; RRID: AB_394082
anti-mouse CD4, BV786 (clone GK1.5)	BioLegend	Cat# 100453; RRID: AB_2565843
anti-mouse CD4, APC-eF780 (clone RM4-5)	eBioscience/ThermoFisher	Cat# 47-0042-82; RRID: AB_1272183
anti-mouse CD4, PerCP-Cy5.5 (clone GK1.5)	BioLegend	Cat# 100434; RRID: AB_893324
anti-mouse CD44, BV605 (clone IM7)	BioLegend	Cat# 103047; RRID: AB_2562451
anti-mouse CD45, BUV563 (clone 30-F11)	BD Biosciences	Cat# 612924; RRID: AB_2870209
anti-mouse CD45, BUV395 (clone 30-F11)	BD Biosciences	Cat# 564279; RRID: AB_2651134
anti-mouse CD48, APC-Cy7 (clone HM48-1)	BioLegend	Cat# 103432; RRID: AB_2561463
anti-mouse CD62L, AF700 (clone MEL14)	eBioscience/ThermoFisher	Cat# 56-0621-82; RRID: AB_494003
anti-mouse CD62L, APC-eF780 (clone MEL-14)	eBioscience/ThermoFisher	Cat# 47-0621-82; RRID: AB_1603256
anti-mouse CD69, BUV737 (clone H1.2F3)	BD Biosciences	Cat# 612793; RRID: AB_2870120
anti-mouse CD8a, BUV395 (clone 53-6.7)	BD Biosciences	Cat# 563786; RRID: AB_2732919

(*Continued on next page*)

Continued

REAGENT or RESOURCE	SOURCE	IDENTIFIER
anti-mouse CD8a, APC (clone 53-6.7)	eBioscience/ThermoFisher	Cat# 17-0081-82; RRID: AB_469335
anti-mouse CD8a, FITC (clone 53-6.7)	eBioscience/ThermoFisher	Cat# 11-0081-85; RRID: AB_464916
anti-mouse CD8a, PerCP-eF710 (clone 53-6.7)	eBioscience/ThermoFisher	Cat# 46-0081-82; RRID: AB_1834433
anti-mouse cKIT/CD117, BV605 (clone 2B8)	BD Biosciences	Cat# 563146; RRID: AB_2738028
anti-mouse cKIT/CD117, PE-Cy7 (clone 2B8)	eBioscience/ThermoFisher	Cat# 25-1171-82; RRID: AB_469644
anti-mouse CTLA-4, PE-Cy7 (clone UC10-AF10-11)	eBioscience/ThermoFisher	Cat# 12-1522-82; RRID: AB_465879
anti-mouse CXCR4, BUV805 (clone 2B11/CXCR4)	BD Biosciences	Cat# 741979; RRID: AB_2871282
anti-mouse F4/80, BUV395 (clone T45-2342)	BD Biosciences	Cat# 565614; RRID: AB_2739304
anti-mouse F4/80, eFluor450 (clone BM8)	eBioscience/ThermoFisher	Cat# 48-4801-82; RRID: AB_1548747
anti-mouse FOXP3, AF647 (clone 150D)	BioLegend	Cat# 320014; RRID: AB_439750
anti-mouse I-A/I-E, FITC (clone M5/114.14.2)	eBioscience/ThermoFisher	Cat# 11-5321-82; RRID: AB_465232
anti-mouse IFNg, PE-Cy7 (clone XMG1.2)	BioLegend	Cat# 505826; RRID: AB_2295770
anti-mouse Ki67, BV786 (clone B56)	BD Biosciences	Cat# 563756; RRID: AB_2732007
anti-mouse Ly6C, eFluor450 (clone HK1.4)	eBioscience/ThermoFisher	Cat# 48-5932-82; RRID: AB_10805519
anti-mouse Ly6C, BV510 (clone HK1.4)	BioLegend	Cat# 128033; RRID: AB_2562351
anti-mouse Ly6G, AF700 (clone 1A8)	BioLegend	Cat# 127622; RRID: AB_10643269
anti-mouse Ly6G, PE (clone 1A8)	BD Biosciences	Cat# 551461; RRID: AB_394208
anti-mouse NKp46, FITC (clone 29A1.4)	eBioscience/ThermoFisher	Cat# 11-3351-82; RRID: AB_1210843
anti-mouse NKp46, PerCP-Cy5.5 (clone 29A1.4)	BioLegend	Cat# 137610; RRID: AB_10641137
anti-mouse PD-1, PE-Cy7 (clone J43)	eBioscience/ThermoFisher	Cat# 25-9985-82; RRID: AB_10853805
anti-mouse PD-L1, PE (clone MIH5)	eBioscience/ThermoFisher	Cat# 12-5982-82; RRID: AB_466089
anti-mouse Sca-1, BV785 (clone D7)	BioLegend	Cat# 108139; RRID: AB_2565957
anti-mouse SiglecF, BV605 (clone E50-2440)	BD Biosciences	Cat# 740388; RRID: AB_2740118
anti-mouse SiglecF, PE (clone E50-2440)	BD Biosciences	Cat# 562068; RRID: AB_10896143
anti-mouse Ter119, PerCP-Cy5.5 (clone TER-119)	BioLegend	Cat# 116228; RRID: AB_893636
anti-mouse TIM-3, BV421 (clone RMT3-23)	BioLegend	Cat# 119723; RRID: AB_2616908
anti-mouse TNFa, AF700 (clone MP6-XT22)	BioLegend	Cat# 506338; RRID: AB_2562918
anti-mouse/human IL-5 PE (clone TRFK5)	BioLegend	Cat# 504303; RRID: AB_315327
anti-human CCR7, APC-R700 (clone 150503)	BD Biosciences	Cat# 565867; RRID: AB_2744304
anti-human CD10, AF700 (clone HI10a)	BD Biosciences	Cat# 563509; RRID: AB_2738247
anti-human CD11c, BV785 (clone 3.9)	BioLegend	Cat# 301644; RRID: AB_2565779
anti-human CD123, PE (clone 6H6)	BioLegend	Cat# 396604; RRID: AB_2801081
anti-human CD138, BV711 (clone MI15)	BioLegend	Cat# 563184; RRID: AB_2738054
anti-human CD14, BUV737 (clone M5E2)	BD Biosciences	Cat# 612763; RRID: AB_2870094
anti-human CD141, BV711 (clone 1A4)	BD Biosciences	Cat# 563155; RRID: AB_2738033
anti-human CD16, BUV496 (clone 3G8)	BD Biosciences	Cat# 612944; RRID: AB_2870224
anti-human CD161, PE-Cy5 (clone DX12)	BD Biosciences	Cat# 551138; RRID: AB_394068
anti-human CD19, PE-Cy5 (clone HIB19)	BD Biosciences	Cat# 555414; RRID: AB_395814
anti-human CD19, BUV395 (clone SJ25C1)	BD Biosciences	Cat# 563549; RRID: AB_2738272
anti-human CD1c, PE Cy7 (clone L161)	BioLegend	Cat# 331516; RRID: AB_2275574
anti-human CD1d, BV786 (clone 42.1)	BD Biosciences	Cat# 743608; RRID: AB_2741620
anti-human CD20, BUV805 (clone 2H7)	BD Biosciences	Cat# 612905; RRID: AB_2870192
anti-human CD24, BB515 (clone ML5)	BD Biosciences	Cat# 564521; RRID: AB_2738834
anti-human CD25, AF647 (clone BC96)	BioLegend	Cat# 302618; RRID: AB_493045
anti-human CD27, PE (clone M-T271)	BD Biosciences	Cat# 555441; RRID: AB_395834
anti-human CD3, PE-Cy5 (clone UCHT1)	BD Biosciences	Cat# 555334; RRID: AB_395741
anti-human CD303, APC-vio770 (clone REA693)	Miltenyi Biotech	Cat# 130-114-178; RRID: AB_2726482
anti-human CD33, PerCP-Cy5.5 (clone WM53)	BioLegend	Cat# 303414; RRID: AB_2074241

(*Continued on next page*)

Continued

REAGENT or RESOURCE	SOURCE	IDENTIFIER
anti-human CD34, FITC (clone 581)	BD Biosciences	Cat# 555821; RRID: AB_396150
anti-human CD38, BUV737 (clone HIT2)	BD Biosciences	Cat# 741837; RRID: AB_2871172
anti-human CD3e, BUV496 (clone UCHT1)	BD Biosciences	Cat# 612940; RRID: AB_2870222
anti-human CD4, BV421 (clone RPA-T4)	BD Biosciences	Cat# 562424; RRID: AB_11154417
anti-human CD41a, BUV395 (clone HIP8)	BD Biosciences	Cat# 740295; RRID: AB_2740034
anti-human CD45RA, BUV737 (clone HI100)	BD Biosciences	Cat# 612846; RRID: AB_2870168
anti-human CD5, PE-Dazzle594 (clone L17F12)	BioLegend	Cat# 364012; RRID:
anti-human CD56, PE-Cy5 (clone B159)	BD Biosciences	Cat# 555517; RRID: AB_395907
anti-human CD66b, AF647 (clone G10F5)	BD Biosciences	Cat# 561645; RRID: AB_10894001
anti-human CD8, BUV805 (clone SK1)	BD Biosciences	Cat# 612754; RRID: AB_2870085
anti-human cKIT/CD117, PE-Cy5.5 (clone 104D2)	Thermofisher	Cat# CD11718; RRID: AB_2536477
anti-human CTLA-4, PE-CF594 (clone BNI3)	BD Biosciences	Cat# 562742; RRID: AB_2737761
anti-human FceRIa, PE-Dazzle594 (clone AER-37(CRA-1))	BioLegend	Cat# 334634; RRID: AB_2571906
anti-human FoxP3, PE-Cy5.5 (clone FJK-16s)	eBioscience/Thermofisher	Cat# 35-5773-82; RRID: AB_11218094
anti-human HLA-DR, BUV661 (clone G46-6)	BD Biosciences	Cat# 612980; RRID: AB_2870252
anti-mouse CD8 (clone 4SM15)	eBioscience/ThermoFisher	Cat# 14-0808-82; RRID: AB_2572861
anti-mouse CD4 (clone 4SM95)	eBioscience/ThermoFisher	Cat# 14-9766-82; RRID: AB_2573008
anti-mouse Foxp3 (clone FJK-16s)	eBioscience/ThermoFisher	Cat# 14-5773-82; RRID: AB_467576
anti-mouse Ly6G (clone 1A8)	BD Biosciences	Cat# 551459; RRID: AB_394206
anti-mouse MBP (clone MT-14.7.3)	Lee Laboratory, Mayo Clinic	N/A
Goat-anti-Rat IgG (clone 3052-08)	Southern Biotech	Cat# 3052-08; RRID: AB_2795846
Purified anti-human CD3 (clone OKT3)	Biolegend	Cat# 317350
Anti-human CD28 (clone CD28.2)	eBioscience/ThermoFisher	Cat# 16-0289-85
Anti-PD1 (Nivolumab)	Bristol-Myers Squibb	N/A
Anti-CTLA4 (Ipilimumab)	Bristol-Myers Squibb	N/A
Biological samples		
KEP tumor fragments	This paper	N/A
Human blood samples from metastatic TNBC patients	This paper	https://clinicaltrials.gov/ct2/show/NCT02499367
Biopsies of metastatic lesions from metastatic TNBC patients	This paper/Netherlands Cancer Institute	https://clinicaltrials.gov/ct2/show/NCT02499367 https://www.nature.com/articles/s41591-019-0432-4
Human blood data from early-stage colon cancer patients	Acquired from principle investigators of NICHE-trial, Netherlands Cancer Institute	https://clinicaltrials.gov/ct2/show/NCT03026140 https://www.nature.com/articles/s41591-020-0805-8
Human blood data from metastatic NSCLC patients, acquired from	Acquired from principle investigators of PEMBRO-RT -trial, Netherlands Cancer Institute	https://clinicaltrials.gov/ct2/show/NCT02492568 https://jamanetwork.com/journals/jamaoncology/fullarticle/2738064
Human blood data from metastatic dMMR cancer patients	Acquired from principle investigators of DRUP-trial, Netherlands Cancer Institute	https://clinicaltrials.gov/ct2/show/NCT02925234 https://www.nature.com/articles/s41586-019-1600-x
Patient-derived tumor fragment data	Acquired from principle investigators of PDTF-platform, Netherlands Cancer Institute	https://www.nature.com/articles/s41591-021-01398-3 https://www.science.org/doi/10.1126/scitranslmed.abj9779

(*Continued on next page*)

Continued

REAGENT or RESOURCE	SOURCE	IDENTIFIER
Chemical, peptides, and recombinant proteins		
IL-33TRAP-C-murine	Gift from R. Beyaert, VIB/UGent	N/A
Recombinant Mouse IL-33	BioLegend	Cat# 580504
Diphtheria Toxin from *Corynebacterium diphtheriae*	Sigma-Aldrich	Cat# D0564-1MG
7-AAD Viability Staining solution	Thermofisher	Cat# 00-6993-50
Ionomycin (calcium salt from Streptomyces conglobatus)	Sigma	Cat# I0634-1mg
Phorbol 12-myristate 13-acetate (PMA)	Sigma	Cat# P1585-1MG
UltraComp eBeads	eBioscience	Cat# 01-2222-42
DNAse I	Invitrogen	Cat# 18068-015
Collagenase A	Roche	Cat# 11088793001
Collagenase IV	Sigma	Cat# C5138-100MG
Liberase TL Research Grade	Roche	Cat# 5401020001
RLT Buffer	Qiagen	Cat# 79216
GolgiPlug	BD Bioscience	Cat# 555029
BD Brilliant stain buffer	BD Bioscience	Cat# 563794
Human FcR Blocking Reagent	Miltenyi	Cat# 130-059-901
Critical commercial assays		
LEGENDplex™ custom mouse panel	BioLegend	N/A
ELISA MAX™ Standard Set Mouse IL-5	BioLegend	Cat# 431201
Fixable Viability Dye eFluor™ 780	eBioscience	Cat# 65-0865-18
Zombie Red Fixable Viability Kit	BioLegend	Cat# 423109
Foxp3/Transcription Factor Staining Buffer Set	Thermofisher	Cat# 00-5523-00
High-capacity cDNA reverse transcription kit	Applied Biosystems	Cat# 4368814
SensiFAST SYBR No-ROX kit	Bioline	Cat# BIO-98020
RNeasy Micro Kit	Qiagen	Cat# 74004
Deposited data		
RNAseq data mouse eosinophils (raw and processed data)	This paper	GEO: GSE210895
RNAseq data of tumor biopsies of TNBC patients treated in the TONIC trial stage I	Netherlands Cancer Institute	EGA: EGAS0001003535 https://www.nature.com/articles/s41591-019-0432-4
RNAseq data of tumor biopsies of TNBC patients treated in the TONIC trial stage II	Netherlands Cancer Institute	Deposit in EGA pending. Available upon request from corresponding author
NanoString data of tumor biopsies of TNBC patients treated in the TONIC trial stage I	Netherlands Cancer Institute	Available upon request from corresponding author
Experimental models: organisms/strains		
Mus musculus: Strain: Wild-type FVB/N	Janvier Laboratories	N/A
Mus musculus: Strain: *K14-cre; Cdh1$^{F/F}$;Trp53$^{F/F}$* (FVB/N)	Netherlands Cancer Institute	N/A
Mus musculus: Strain: *Rag-1$^{-/-}$* (FVB/N)	Gift from L. Coussens	N/A
Mus musculus: Strain: *Cdh1$^{F/F}$; Trp53 $^{F/F}$;Foxp3$^{GFP\text{-}DTR}$* (FVB/N)	Netherlands Cancer Institute	N/A
Oligonucleotides		
TGGGGGTACTGTGGAAATGC (mouse IL-5 FW 1)	Integrated DNA Technologies	N/A
CCACACTTCTCTTTTTGGCGG (mouse IL-5 RV1)	Integrated DNA Technologies	N/A

(*Continued on next page*)

Continued

REAGENT or RESOURCE	SOURCE	IDENTIFIER
CAAGCAATGAGACGATGAGGC (mouse IL-5 FW 2)	Integrated DNA Technologies	N/A
AGCATTTCCACAGTACCCCC (mouse IL-5 RV 2)	Integrated DNA Technologies	N/A
AGGTCGGTGTGAACGGATTTG (mouse GAPDH FW)	Integrated DNA Technologies	N/A
TGTAGACCATGTAGTTGAGGTCA (mouse GAPDH RV)	Integrated DNA Technologies	N/A
TGGAGCTGCCTACGTGTATG (human IL-5 FW)	Integrated DNA Technologies	N/A
TTCGATGAGTAGAAAGCAGTGC (human IL-5 RV)	Integrated DNA Technologies	N/A
GGAGCGAGATCCCTCCAAAAT (human GAPDH FW)	Integrated DNA Technologies	N/A
GGCTGTTGTCATACTTCTCATGG (human GAPDH RV)	Integrated DNA Technologies	N/A
Software and algorithms		
FlowJo v10.6.2	BD Biosciences	https://www.flowjo.com/solutions/flowjo
GraphPad Prism v8.4.3	GraphPad/Dotmatics	https://www.graphpad.com/scientific-software/prism/
SPSS Statistics v24	IBM	https://www.ibm.com/support/pages/downloading-ibm-spss-statistics-24
LEGENDplex™ Data Analysis Software Suite	BioLegend	https://www.biolegend.com/en-us/legendplex/software
GSEA v4.0.3	Broad Institute	https://www.gsea-msigdb.org/gsea/index.jsp
Qlucore Omics Explorer	Qlucore	https://qlucore.com/omics-explorer
Hisat2	Kim et al, *Nature Biotechnology*, 2019	http://daehwankimlab.github.io/hisat2/
STAR v2.7.1a	Dobin et al., *Bioinformatics* 2013[79]	https://github.com/alexdobin/STAR
Deseq2 v1.24.0	Love et al, *Genome Biology* 2014[80]	https://bioconductor.org/packages/release/bioc/html/DESeq2.html
Python v3.7.6	Python	https://www.python.org/downloads/release/python-376/
Pandas v1.0.1	McKinney, 2010 Pandas, 2020[81]	https://pandas.pydata.org/
NumPy v1.18.1	Harris et al., *Nature* 2020[83]	https://numpy.org/
Matplotlib v3.1.3	Hunter et al., *Computing in Science and Engineering* 2007[84]	https://matplotlib.org/
Seaborn v0.10.0	Waskom et al., 2017[85]	https://seaborn.pydata.org/
Statannot v0.2.2	Weber, 2020[86]	https://github.com/webermarcolivier/statannot
Ggplot2 v3.3.5	Wickham, *ggplot2: Elegant Graphics for Data Analysis* 2016[93]	https://github.com/tidyverse/ggplot2
Ggpubr v0.4.0	Kassambara, *ggpubr: 'ggplot2' Based Publication Ready Plots*, 2020[94]	https://github.com/kassambara/ggpubr

(*Continued on next page*)

Continued

REAGENT or RESOURCE	SOURCE	IDENTIFIER
Ggrepel v0.9.1	Slowikowski, *ggrepel: Automatically Position Non-Overlapping Text Labels with 'ggplot2'*, 2021[95]	https://CRAN.R-project.org/package=ggrepel
Reshape2 v1.4.4	Wickham, *Reshaping Data with the {reshape} Package*, 2007[96]	http://www.jstatsoft.org/v21/i12/
Dplyr v1.0.8	Wickham et al., *dplyr: A Grammar of Data Manipulation*, 2022[97]	https://CRAN.R-project.org/package=dplyr
Purrr v0.3.4	Henry et al., *purrr: Functional Programming Tools*, 2020[98]	https://CRAN.R-project.org/package=purrr
Heatmap3 v1.1.9	Zhao et al., *heatmap3: An Improved Heatmap Package*, 2021[99]	https://CRAN.R-project.org/package=heatmap3
Ggbeeswarm v0.6.0	Clarke et al., *ggbeeswarm: Categorical Scatter (Violin Point) Plots*, 2017[100]	https://CRAN.R-project.org/package=ggbeeswarm

RESOURCE AVAILABILITY

Lead contact

Requests for further information and resources of this study should be directed to Karin de Visser (k.d.visser@nki.nl)

Materials availability

This study did not generate new unique reagents.

Data and code availability

- RNA-sequencing data on mouse eosinophils generated in this study has been deposited at Gene Expression Omnibus (GEO) under accession number GSE210895 and are publicly available from the date of publication. RNA-sequencing data on tumor biopsies of TNBC patients treated in the TONIC-trial stage 1 are deposited at the European Genome-phenome Archive (EGA) under accession number EGAS0001003535 and will be made available from the corresponding author on reasonable request. NanoString data from TONIC-trial stage 1 and RNAseq data of TNBC patients treated in TONIC-trial stage 2 reported in the paper are not deposited in a public repository pending ongoing work but can be made available from the corresponding authors upon reasonable request. All human data requests will be reviewed by the Institutional Review Board (IRB) of the NKI and applying researchers have to sign a data transfer agreement after IRB approval before the data can be released.
- This paper does not report original code.
- Any additional information required to re-analyze the data reported in this paper is available from the lead contact upon request.

EXPERIMENTAL MODEL AND SUBJECT DETAILS

Preclinical models

The transgenic *Keratin14-cre;Cdh1$^{F/F}$;Trp53$^{F/F}$* (KEP) model for primary mammary tumorigenesis[34] (FVB/N genetic background), KEP-based orthotopic mammary tumor model and the KEP-based model for spontaneous breast cancer metastasis[35] were used as previously described.[26,27] Female KEP mice were monitored twice per week for spontaneous tumor formation by palpation starting at the age of 3.5 months. KEP mice develop palpable tumors between 6 and 8 months of age.[34] The perpendicular diameters of the tumors were measured using a caliper and tumor area was calculated accordingly. Female FVB/N mice of 8–12 weeks of age were obtained from Janvier Labs. *Rag1* k.o. in FVB/N genetic background were a gift from L. Coussens.[74] *Cdh1$^{F/F}$;Trp53$^{F/F}$;Foxp3$^{DTR-GFP}$* mice[75] in FVB background were generated by the Animal Modeling Facility (AMF) of the Netherlands Cancer Institute. All mice were kept in individually ventilated cages at the animal laboratory facility of the NKI. Food and water were provided *ad libitum*. All animal experiments were approved by the Animal Ethics Committee of the NKI and performed in compliance with the national and European guidelines for animal care and use.

Clinical trial procedures

Trial procedures were performed as described previously in the respective publications.[28–31] All patients included in stage 1[28] and stage 2 of the TONIC-trial (NCT02499367) were included in the current analysis. In stage 1, 70 patients were included in the TONIC-trial, of which 67 patients received nivolumab and were available for efficacy and translational analysis, as previously described.[28] An additional 47 patients were included in stage 2 of the trial, of which 44 patients received nivolumab and were available for efficacy and translational analysis. From these 111 patients (Table S1), paired flow cytometry on fresh blood (baseline, after two-week induction period and after 3 cycles of nivolumab) was performed on 55 patients and paired routine eosinophil counts were available for 90

patients (sample availability in Table S2 and Figure S1B). Progression-free survival was measured as time between date of randomization and date of progression according to iRECIST or date of death. Overall survival was measured as time between first date of nivolumab and date of last follow-up or date of death. Data was cut-off at 1 March 2021.

Patients with metastatic NSCLC were treated in the PEMBRO-RT trial (NCT02492568)[29] at the NKI (paired data for n = 40 from the total of 55 patients treated at the NKI and the total of 76 patients included in the trial), in which patients were randomized to pembrolizumab with or without upfront radiation.[29] To investigate eosinophil dynamics in patients with metastatic dMMR tumors, we made use of patients treated with nivolumab in the NKI within the dMMR cohort (paired data for n = 9 of the total 11 patients treated at the NKI and the total of 30 patients included in the cohort) of the DRUP-trial (NCT02925234).[31] Finally, patients with early-stage colon cancer (either dMMR (n = 21) or pMMR (n = 17)) were treated in the NICHE-trial, in which patients are treated with neo-adjuvant ipilimumab (1 mg/kg) and nivolumab (3 mg/kg), with or without additional celecoxib in pMMR patients (NCT03026140).[30] In the patients with metastatic disease, response was defined as complete response (CR), partial response (PR) and stable disease (SD) of at least 24 weeks, defined according to RECIST1.1.[76] Best overall response in the TONIC-trial was measured according to iRECIST.[77] Response in the NICHE-trial was defined as any pathological response (>10% tumor regression), assessed on surgical material after neo-adjuvant treatment. All clinical study protocols were approved by the medical-ethical committee of the NKI and conducted in accordance with the ICH Harmonized Tripartite Guideline for Good Clinical Practice and the principles of the Declaration of Helsinki. All patients provided written informed consent to participate in the clinical trial.

METHOD DETAILS

Preclinical intervention studies

In the spontaneous KEP model, all treatments started when tumor area reached 50 mm^2. For the KEP-based orthotopic mammary tumor model, mammary tumor pieces of 1 mm^2 size derived from KEP mice were orthotopically transplanted into the mammary glands of female FVB/N mice. In this model, treatments started when tumor area reached 25 mm^2. For the survival experiments and endpoint analysis mice were sacrificed when the cumulative tumor burden reached 225 mm^2. KEP mice were sacrificed 21 days after initiation treatment to analyze the 'responsive phase' or at a tumor size of 150mm^2 for the KEP-based orthotopic mammary tumor model. Cisplatin (Accord Healthcare Limited) was injected intravenously once every two weeks at 5 mg/kg, for a maximum of 4 cycles. Anti-mouse PD-1 (RMP1-14, BioXCell), anti-mouse CTLA-4 (9D9, BioXCell) or control (2A3, BioXCell) antibodies were each given intraperitoneally at 100 μg per mouse, twice per week. Anti-CD8 (2.43, BioXCell) or anti-CD4 (GK1.5, BioXCell) antibody were given intraperitoneally at 200 μg per mouse, twice per week. Anti-mouse SiglecF (238047, R&D systems) and control antibody (2A3, BioXCell) were administered intraperitoneally at 20 μg per mouse, three times a week. Anti-IL-5 (TRFK5, BioXCell) and control antibody (HRPN, BioXCell) were given intraperitoneally at 500 μg per mouse, twice per week. Recombinant mouse IL-33 (Biolegend) was given intraperitoneally at 0.4 μg per mouse, three times a week. IL-33-TRAP (provided by Rudi Beyaert laboratory, VIB, Belgium) was given intraperitoneally at 50 μg per mouse daily. For the T_{reg} depletion in *Foxp3-GFP-DTR* mice, DT (Diptheria toxin from *Corynebacterium diphteriae*) was given intraperitoneally at 25 μg/kg, at day 0 and day 4 after start of treatment. All antibody treatments continued until the experimental endpoint was reached.

For metastasis experiments, mammary tumor pieces of 1mm^2 size derived from KEP mice were orthotopically transplanted into the mammary glands. Mammary tumors were surgically removed when they reached the size of 100 mm^2. In the metastasis experiments, all treatments started 15 days after mastectomy, when all mice have established metastasis in the lung and/or lymph node, and treatments continued until the experimental endpoint. All treatments were performed as described above. For survival experiments, mice were sacrificed when they developed signs of distress caused by metastatic disease (respiratory distress) or when lymph node metastasis reached the size of 225 mm^2. For analysis of 'responsive phase', metastasis-bearing mice were sacrificed 10 days after start of treatment for Ctrl Ab and ICB groups and 21 days for CIS + Ctrl Ab and CIS + ICB groups.

Flow cytometry analysis

Tumors and organs from KEP mice and FVB/N mice with metastatic breast cancer were collected in ice-cold PBS. Blood was withdrawn by tail vein or heart puncture and collected in K_2EDTA-containing tubes (BD Microtainer Blood Collection Tubes). Tumor tissues and lungs were mechanically minced using the McIlwain tissue chopper (Mickle Laboratory Engineering) and enzymatically digested at 37°C in DMEM medium containing 3 mg/mL collagenase type A (Roche) plus 25 μg/mL of DNase I (Sigma) for 45 min or in 100 μg/mL Liberase TM (Roche) for 30 min, respectively. Half of the lymph nodes and spleen were enzymatically digested in RPMI medium containing 3 mg/mL collagenase type IV (ThermoFisher Scientific), 2 mM $CaCl_2$, 2% FCS and 25 μg/mL DNase I for 30 min at 37°C and used to stain for myeloid cell populations. The other half was directly processed into single cell suspensions and used for lymphoid cell panels. All digestion reactions were stopped by adding cold DMEM medium containing 10% FCS. For the analysis of bone marrow, tibia and femurs were flushed with PBS and processed as the other organs. Single-cell suspensions were obtained by mashing through 70 μm filter and resuspended in PBS containing 0.5% BSA (Roche) and 2 mM EDTA (Lonza). Blood, spleen, lungs and bone marrow samples were treated for 5 min at room temperature with NH_4 lysis buffer to remove erythrocytes.

For flow cytometry analysis of patient sample preparations, peripheral blood was collected in an K_2EDTA vacutainer (BD) and processed and analyzed within 24 h. Red blood cells were lysed (lysis buffer: dH_2O, NH_4Cl, $NaHCCO_3$, EDTA) and cells were resuspended in PBS containing 0.5% BSA and 2 mM EDTA. To obtain absolute white blood cell counts per mL of human blood, the total

post-lysis cell count was obtained using the NucleoCounter NC-200 (Chemometec) Automated cell counter was divided by the total volume (mL) of blood.

For intracellular cytokine staining, cells were stimulated *ex vivo* with 50 ng/mL PMA, 1 μM ionomycin and Golgi-Plug (1:1000; BD) for 3 h at 37°C in IMDM medium supplemented with 8% FCS, 100 IU/mL Penicillin-Streptomycin (Roche) and 0.5% β-mercaptoethanol. For surface antigen staining, cells were first incubated with rat anti-mouse CD16/CD32 antibody (1:100; Mouse Fc Block, BD Bioscience) or human FcR Blocking Reagent (1:100 Miltenyi) for 15 min at 4°C and then incubated with fluorochrome-conjugated antibodies for 30 min at 4°C, in the dark. For intracellular antigen staining, cells were fixed with Fixation/Permeabilization solution 1X (Foxp3/Transcription Factor Staining Buffer Set, eBioscience) for 30 min at 4°C and stained with fluorochrome-conjugated antibodies in Permeabilization buffer 1X (eBioscience) for 30 min at room temperature. Viability was assessed by staining with either 7AAD staining solution (1:20; eBioscience), Zombie Red Fixable Viability Kit (1:800 BioLegend) or with Fixable Viability Dye APC-eFluor780 (1:1000; eBioscience). Data acquisition was performed on BD LSRII flow cytometer using Diva software (BD Biosciences) and data analysis was performed using FlowJo software version 10.6.2. All used flow cytometry antibodies can be found in key resources table. Gating strategies are displayed in Figures S8 and S9.

Immunohistochemistry

KEP tumors were fixed for 24 h in 10% neutral buffered formalin, embedded in paraffin and sectioned at 4 μm. CD4, CD8, FOXP3 and Ly6G stainings were performed by the Experimental Animal Pathology facility of the NKI. Antibodies are listed in key resources table. For MBP staining, sections were deparaffinized in xylene for 20 min, rehydrated, and incubated with 3% H_2O_2 for 10 min at room temperature. Antigen retrieval was performed using Pepsin solution (ThermoFischer Scientific) for 10 min at room temperature. As blocking solution PBS with 2.5% BSA and 10% normal goat serum was used for 30 min at room temperature. Sections were incubated with rat anti-mouse MBP antibody (1:350, clone MT-14.7.3, Lee Laboratory, Mayo Clinic) diluted in 0.5X blocking solution, overnight at 4°C. Biotinylated goat anti-rat IgG antibody (1:300, Southern Biotech) was used as secondary antibody. Streptavidin-HRP and DAB solution (DAKO) were used following manufacturer's instructions. Sections were counterstained with hematoxylin solution. Slides were scanned using Aperio ScanScope and analyzed with Aperio ImageScope software version 12.4.3 (Aperio, Vista).

RNA-sequencing of mouse eosinophils

For the transcriptomic analysis, a minimum of 35000 eosinophils ($CD11b^+$ $Ly6G^{low}$ SSC^{high} $F4/80^+$) were sorted from the blood in RLT buffer containing 1% β-ME, using a BD FACSAria™ Fusion Cell Sorter. RNA was isolated following RNeasy Mini Kit (Qiagen) protocol, using 80% ethanol instead of RPE buffer. Smart-seq2 library preparation was performed as previously described,[78] using 2100 Bioanalyzer System (Agilent) for quality control. Only samples with RIN ≥ 7 were used for RNA-sequencing analysis. The strand-specific reads (65 bp single-end) were sequenced with the HiSeq 2500 System (Illumina). Demultiplexing of the reads was performed with Illumina's bcl2fastq software and demultiplexed reads were aligned against the mouse reference genome (build 38) using HISAT2. HISAT2 was supplied with known set of gene models (Ensembl version 87). Qlucore Omics Explorer (Qlucore AB, Lund, Sweden) software was used to calculate and visualize differentially expressed genes ($p < 0.05$) and sample variation, after having discarded genes with fewer then 30 mapped reads in at least 9 samples and performed data normalization by TMM method. Gene set enrichment analysis (GSEA) was performed using the GSEA program version 4.0.3 (Broad Institute). Hallmarks gene sets from Molecular Signatures Database v7.2 were used. Mouse gene symbols were remapped to human orthologues using Mouse_Gene_Symbol_Remapping_Human_Orthologs_MSigDB.v7.2.chip annotation file.

Cytokine analysis

For the analysis of cytokines and chemokines expression in mouse plasma, serum or tumor lysate, custom-made Legend Plex bead-based immunoassay (Biolegend) was used, according to manufacturer instructions. 50 μg of total protein from lysed tissues was used for measurements. Data acquisition was performed on LSRFortessa (BD Biosciences) flow cytometer using Diva software (BD Biosciences) and analyzed using LEGENDplex™ Data Analysis Software Suite (Biolegend). In addition, mouse IL-5 ELISA detection kit (BioLegend) was used, according to manufacturer instructions.

Routine eosinophil counts in patient cohorts

Eosinophil counts were measured with an XN-2000 Hematology Analyzer of Sysmex at the diagnostic Clinical Chemistry Department. The variation coefficient was below 10%.

RNA extraction and NanoString gene expression analysis

RNA was isolated from freshly frozen sections of biopsies as previously described.[28] For each patient, sequential biopsies were taken from the same metastatic lesion, however per patient, the site of the metastatic lesion was different (predominantly, but not only, lymph nodes, recurrent lesion in breast, liver, skin). mRNA expression was measured with the nCounter technology provided by NanoString Technologies as previously described.[28] NanoString mRNA counts were available for patients included in stage 1 of the TONIC-trial (paired metastatic biopsies pre-nivolumab and on-nivolumab n = 26).

RNA-sequencing on patient tumor biopsies

The RNA-sequencing data was aligned to the reference genome GRCh38 with STAR (version 2.7.1a)[79] with two-pass mode option set to "Basic". For comparison between patients, a median of ratios normalization was performed with Deseq2 R package (version 1.24.0,[80]) and for within-patient comparisons TPM normalization was used. Data was analyzed using Python 3.7.6, with pandas (version 1.0.1,[81,82]) and NumPy (version 1.18.1,[83] packages. Plots were created using Matplotlib (version 3.1.3,[84]) and Seaborn (version 0.10.0,[85]), statistical annotation was added using statannot (version 0.2.2,[86]). All gene-signatures are listed in Table S3.[87–92] Mean normalized expression values of individual genes were taken as a signature score. A fold change of the signature score baseline vs. on-nivolumab was taken for each signature. RNA-sequencing on paired metastatic lesions (baseline and on-nivolumab) was available for 48 patients, included in both stages of the trial.

RT-qPCR

Human $CD3^+$ $CD4^+$ T cells were sorted from TONIC patient PBMCs into RLT buffer containing 1% β-ME, using a BD FACSAria™ Fusion Cell Sorter. RNA was isolated following RNeasy Micro Kit (Qiagen) protocol. RNA was converted to cDNA with an AMV reverse transcriptase using Oligo(dT) primers (Invitrogen). For mouse $CD4^+CD25^-$ T cells, RNA was converted to cDNA using High-capacity cDNA reverse transcription kit (ThermoFisher Scientific), following kit instructions. cDNA (20 ng per well) was analyzed by SYBR green real-time PCR with 500 nM primers using a LightCycler 480 thermocycler (Roche). *Gapdh* was used as a reference gene. Primer sequences used for each gene are listed in the key resources table. Fold change in expression was calculated using $2^{-(\Delta Ct.x\ -\ average(\Delta Ct.control))}$.

Human PBMC stimulation

PBMCs were isolated at baseline from patients with metastatic TNBC in the control arm of the TONIC trial. Patient PBMCs were seeded at a density of 500,000 cells per well in 96-well plates in DMEM (Sigma), 10% FBS (Sigma), 1 mM sodium pyruvate (Sigma), 1x MEM nonessential amino acids (Sigma), 1x Glutamax, 100 ng/mL penicillin/streptomycin, 50 nM 2-mercaptoethanol (Sigma). Cells were stimulated with a suboptimal concentration of 0.5 μg/mL plate bound anti-CD3 (OKT3, BioLegend) and 2 μg/mL anti-CD28 (28.2, eBioscience) for 48 h. Anti-PD1 (Nivolumab,10 μg/mL) was added where indicated. GolgiPlug was added to each well for the final 4 h of stimulation and cells were analyzed by flow cytometry as described above.

PDTF culture and stimulation

PDTF cultures were performed as described previously.[45,46] Briefly, tumor samples were collected from surgical material of patients with renal cell carcinoma (anti-PD1+anti-CTLA-4 treated n = 1 & anti-PD1 treated n = 2), ovarian cancer (n = 4 & n = 1), melanoma (n = 7 & n = 5), non–small cell lung cancer (n = 1 & n = 3), and colorectal cancer (n = 0 & n = 1). Patient characteristics were described previously for samples stimulated with aPD-1 & aCTLA-4[46] and listed in Table S4 for samples stimulated with aPD-1. Definition of responder and non-responder PDTFs were described previously.[45,46] Samples were cut in fragments of 1–2 mm^3 and embedded in an artificial extracellular matrix in a 96-well plate. PDTF cultures were stimulated with medium supplemented with either anti-PD1 alone (nivolumab, Bristol-Myers Squibb) at 10 μg/mL or anti-PD-1 plus anti-CTLA4 (ipilimumab, Bristol-Myers Squibb) at 10 μg/mL where indicated. After 48 h of culture at 37°C, supernatants were collected and IL-5 levels were measured using the LEGENDplex Human Th Cytokine (BioLegend), according to the manufacturer's protocol.

QUANTIFICATIONS AND STATISTICAL ANALYSIS

Statistical analysis was performed in GraphPad Prism (version 8.4.3) or SPSS Statistics (version 24). All statistical tests were two-sided. All p values are uncorrected for multiple testing unless stated otherwise. For heatmaps of human flow cytometry data (Figures S1C–S1F), log_2 transformed cell count/mL or log_2 transformed fold change were depicted, centered around the median for each population (row) separately. Hierarchical clustering was performed on populations and patients based on 1 minus Pearson correlation and Euclidian distance respectively. Complete-linkage was used for both cell populations and patients. To assess dynamics in each cell population analyzed by flow cytometry between baseline and on-nivolumab, the median log_2 fold change from baseline to on-nivolumab (log_2(on-nivolumab) – log_2(pre-nivolumab) was plotted against Benjamini-Hochberg corrected p values (Figure 1B). For dynamics in each cell population analyzed by flow cytometry between pre-nivolumab and on-nivolumab, linear modeling was performed (similar to a two-way ANOVA) to predict log_2 fold changes between pre-nivolumab and on-nivolumab counts/mL based on response and induction treatment:

Log_2-fold_change ~ response + induction_treatment

This model assumes that the response and induction treatment have an additive and independent effect on log fold changes. For each population responders were contrasted from non-responders. For Figure S2D, the regression coefficients associated with response for each population (x axis) against the associated (Benjamini-Hochberg corrected) p values (Wald-test) were plotted. The uncorrected (Wald-test) p values associated with different induction treatments were estimated. For each population we performed a Shapiro-Wilk normality test on the regression residue to see if the normality assumption was violated.

ADDITIONAL RESOURCES

This paper included flow cytometry and hemocytometer data of blood samples and RNAseq data of tumor biopsies from patients with metastatic TNBC treated in the Netherlands Cancer Institute in the TONIC-trial (NCT02499367). This paper also included hemocytometer data on blood samples generated in the Netherlands Cancer Institute from patients with metastatic NSCLC treated in the PEMBRO-RT trial (NCT02492568), patients with metastatic dMMR tumors treated in the DRUP-trial (NCT02925234), and patients with early-stage colon cancer treated in the NICHE-trial (NCT03026140). Data were kindly provided by the principal investigators of the clinical trials. Further information on the clinical trial procedures and links to clinical publications can be found in the Methods section on clinical trial procedures and key resources table.